Distribution Agreement

In presenting this thesis as a partial fulfillment of the requirements for a degree from Emory University, I hereby grant to Emory University and its agents the non-exclusive license to archive, make accessible, and display my thesis in whole or in part in all forms of media, now or hereafter now, including display on the World Wide Web. I understand that I may select some access restrictions as part of the online submission of this thesis. I retain all ownership rights to the copyright of the thesis. I also retain the right to use in future works (such as articles or books) all or part of this thesis.

George Cheng April 1, 2022

Explorations of Peptide Self-Assembly in Three Chapters

By

George Cheng

Dr. Vincent Conticello
Advisor

Department of Chemistry

Dr. Vincent Conticello
Advisor

Dr. Richard Himes
Committee Member

Dr. Kate O'Toole
Committee Member

2022

Explorations of Peptide Self-Assembly in Three Chapters

By

George Cheng

Dr. Vincent Conticello
Adviser

An abstract of
a thesis submitted to the Faculty of Emory College of Arts and Sciences
of Emory university in partial fulfillment
of the requirements of the degree of
Bachelor of Science with Honors

Chemistry

2022

Abstract:

Explorations of Peptide Self-Assembly in Three Chapters

By George Cheng

The study of biocompatible materials with implications in drug delivery, protein design and modification, and modelling of natural processes occupies a valuable niche at the intersection of many chemical, biological, and physical disciplines. Biological macromolecules are unique for their complex and intrinsic tendency to self-assemble into supramolecular morphologies that impart unique properties from linear sequences of disorganized building blocks. Access to higher order organization of peptide and peptidomimetic nanostructures begins with an understanding of the diverse set of secondary structural characteristics that can emerge from even the simplest sequences of amino acids. This work explores self-assembling peptides with design motifs based on α-helical miniproteins, polymorphic amphiphilic β-sheets, and the unique properties of β-peptide foldamers. Using a variety of biophysical techniques to optimize and delineate the properties of self-assembled oligomers, it is possible to identify trends in the sequence of synthetic polypeptides that affect resulting structure. The sequence to structure correlation of peptide nanomaterials offers insight into the quandary of the protein-folding problem and generates new tools for understanding the natural order of living systems.

Explorations of Peptide Self-Assembly in Three Chapters

By

George Cheng

Dr. Vincent Conticello

Adviser

A thesis submitted to the Faculty of Emory College of Arts and Sciences

of Emory University in partial fulfillment

of the requirements of the degree of

Bachelor of Science with Honors

Chemistry

2022

Acknowledgements:

I would first like to express my deepest gratitude to Dr. Vincent Conticello who has played an invaluable part of my undergraduate experience beginning with my first semester of general chemistry. He welcomed me to his research group with open arms and entrusted me with a diverse portfolio of remarkable projects. Dr. Conticello's overwhelming intellect and inextinguishable curiosity are matched only by his genuine commitment and kindness towards the members of his group. It is no exaggeration to say that he is the primary reason I choose to study chemistry.

I would also like to thank the group members that I have grown up with during my four years in the Conticello lab. My graduate mentor Ordy Gnewou has been an exceptional role model and friend. Her unparalleled work ethic has pushed me to learn and grow both academically and interpersonally. I would also like to acknowledge Duong Nguyen and Jessalyn Rogers who have gone out of their way to accommodate and mentor me since I first joined. Our research group is not large, and yet I have never been alone.

I would also like to thank the members of the lab that have already graduated from our group, Dr. Sheng Wang and Dr. Andrea Merg who collectively trained, guided, and taught the current members of the lab. The precedents and protocols they wrote have set a high standard for our work.

Lastly, I would like to thank Dr. Ricardo Guerrero-Ferreira for his guidance and training on use of the various electron microscopy technology available in the Robert. P. Apkarian Integrated Electron Microscopy Core, Dr. David Lynn for allowing us to borrow his laboratory space and equipment for peptide synthesis, and Dr. Monika Raj for allowing us to use her mass spectrometry machine.

Table of Contents

Introduction:

Peptide nanomaterials represent an intriguing and valuable niche in the realm of material science. The building blocks of biological systems that have evolved under stringent selective pressures are diverse, easily modulated, and obey strict architectural paradigms[1,2]. The ground-up *de novo* design of oligopeptides that take inspiration from motifs found in complex natural proteins and peptides allows the isolation, optimization, and study of individual paradigms in protein folding. These novel materials offer incredible potential for unnaturally designed structural morphologies that remain biocompatible[3-8].

A relevant example of a recurring pattern that emerges in self-assembling systems at multiple organizational levels is the propensity of asymmetric units to form helices. Virtually all secondary structures can be represented by their helical properties, including β-sheets which can be thought of as helices with two residues per turn. As early as the 1943 it was realized that repeating hydrogen-bonding and Van der Waal interactions in the structurally equivalent main chain of all peptides fundamentally encourages the formation of helical secondary structures even before side chain interactions are considered[9].

At higher levels of organization, proteins and peptides monomers will form helical suprastructures if interactions between the monomers are not symmetric along a planar ring. Any translation or rotation of the binding interactions along a third dimension will result in a helix, and so even large, irregular, and globular proteins have a tendency to form helical suprastructures when treated as a monomeric unit[10]. Oligopeptides can be designed to self-assemble from polypeptide chains into a diverse range of versatile and programmable tertiary and quaternary structures. This makes peptide oligomer systems extremely attractive in the realm

of material science for producing a wide range of architecturally disparate nanostructures with tunable properties.

Beyond the scope of natural amino acids lies a burgeoning field of biomimetic foldamers[11]. The potential for new classes of biocompatible building blocks to produce novel folding motifs and structures with predictable properties is especially important in the context of *de novo* peptide design. Unlocking new tools for advanced synthesis and design of hierarchical assembly through molecules that are designed to fold compactly relieves that burden associated with limitations in our understanding of protein folding.

The underlying theme of this thesis is the characterization of self-assembling synthetic oligopeptides which exploit naturally occurring and *de novo* designed supramolecular folding regimes. The purpose of each project was to explore existing rules in peptide design, as well as to elucidate new structural elements that emerge with modification of understood peptide sequences and assembly conditions.

References:

1. Lu, Y., & Freeland, S. (2006). On the evolution of the standard amino-acid alphabet. Genome biology, 7(1), 102. https://doi.org/10.1186/gb-2006-7-1-102
2. Dill, K. A., Ozkan, S. B., Shell, M. S., & Weikl, T. R. (2008). The protein folding problem. Annual review of biophysics, 37, 289–316. https://doi.org/10.1146/annurev.biophys.37.092707.153558
3. Hamley IW. Nanotechnology with soft materials. Angew Chem Int Ed Engl. 2003 Apr 17;42(15):1692-712. doi: 10.1002/anie.200200546. PMID: 12707884.
4. Yadav, P. Yadav, H. Shah, V.G., Shah, G. Dhaka, G.(2015).Biomedical Biopolymers, their Origin and Evolution in Biomedical Sciences: A Systematic Review,J Clin of Diagn Res. 9(9), ZE21-ZE25.
5. Aksakal, R., Mertens, C., Soete, M., Badi, N., Du, F., Applications of Discrete Synthetic Macromolecules in Life and Materials Science: Recent and Future Trends. Adv. Sci. 2021, 8, 2004038. https://doi.org/10.1002/advs.202004038
6. Galit Fichman, Ehud Gazit, Self-assembly of short peptides to form hydrogels: Design of building blocks, physical properties and technological applications, Acta Biomaterialia, Volume 10, Issue 4, 2014, Pages 1671-1682, ISSN 1742-7061, https://doi.org/10.1016/j.actbio.2013.08.013.
7. Conticello V., Hughes S., Modlin C. (2017) Biomaterials Made from Coiled-Coil Peptides. In: Parry D., Squire J. (eds) Fibrous Proteins: Structures and Mechanisms. Subcellular Biochemistry, vol 82. Springer, Cham. https://doi.org/10.1007/978-3-319-49674-0_17

8. Gao, X., & Matsui, H. (2005). Peptide-Based Nanotubes and Their Applications in Bionanotechnology. Advanced materials (Deerfield Beach, Fla.), 17(17), 2037–2050. https://doi.org/10.1002/adma.200401849
9. The Structure of Fibrous Proteins. Maurice L. Huggins Chemical Reviews 1943 32 (2), 195-218 DOI: 10.1021/cr60102a002
10. Egelman EH. A tale of two polymers: new insights into helical filaments. Nat Rev Mol Cell Biol. 2003 Aug;4(8):621-30. doi: 10.1038/nrm1176. PMID: 12923524.
11. Foldamers: A Manifesto, Samuel H. Gellman, Accounts of Chemical Research 1998 31 (4), 173-180, DOI: 10.1021/ar960298r

Chapter 1: Synthesis of Peptide-Miniprotein Conjugates

Introduction and Design:

When faced with the daunting task of rationalizing the sequence to structure relationship of large proteins and supramolecular assemblies, it is possible to simplify the problem through retro-analysis of model systems. In the Protein Database (PDB) there are more than 188,000 macromolecules entered, of which only 7% are <100 residues in length[1]. For larger systems, the overlapping interactions of various folding regimes, non-covalent and covalent interactions, and binding of other proteins, ligands, and ions introduces far too many variables to reliably study. One means of isolating individual folding patterns is by using short (<50 residue) protein models which still have well-defined cooperative folding and contain hydrophobic cores. These so-called "miniproteins" are distinguished from other small peptides that fold into ordered states because they display hydrophobic cores much like larger complex globular proteins[2].

The polyproline-II-loop-α-helix fold motif was first identified in avian pancreatic polypeptide (aPP), a 36-residue hormone which packs two distinct secondary structures to generate a hydrophobic core[3]. aPP is one of the quintessential predecessors of modern miniprotein research because it folds into a well-structured dimer stabilized entirely by noncovalent interactions. The polyproline-II-loop-α-helix fold is stabilized by interdigitation of prolines on the left-handed polyproline-II type helix with tyrosines on the α-helix to form a distinctive hydrophobic core.

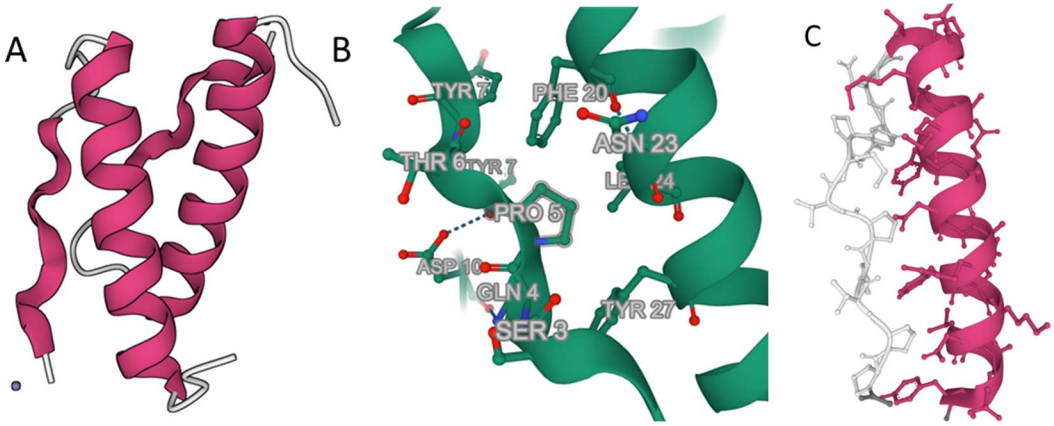

Figure 1. Crystal structure of aPP dimer solved at 1.4 angstrom resolution **(A)** Ball and stick representation of the interdigitation of the polyproline helix and adjacent aromatic residues on the α-helix in aPP **(B)** (PDB: 1PPT, from Blundell et al.[3]) NMR Spectroscopy derived structure of PPα showing the KIH packing and CH-π interactions **(C)** (PDB: 5LO2, from Baker et al.[5])

aPP and aPP mutants have seen use in the development of miniprotein therapeutics and as scaffolds for DNA and protein surface binding recognition epitopes[4]. The polyproline-II-loop-α-helix architecture also represents a flexible design template with a simple and well-understood folding regime. The Woolfson group has worked extensively with this template to design a series of short peptides, PPα, which fold into stable monomers with an amphipathic α-helix taken from the surface adhesin and antigen (AgI/II) of *Streptococcus Mutans* and a polyproline-II helix and loop derived from bovine pancreatic polypeptide hormone[5,6]. PPα and its mutants are designed to be monomeric by maximizing knobs-in-holes (KIH) type interactions of prolines and various aromatic sidechains of variable electron deficiency. Although KIH interactions are traditionally

used to describe the packing of α-helices in coiled coils, the analogy is useful in describing the tight fitting of hydrophobic residues on PPα which are driven by CH- π interactions.

The Conticello group has worked extensively on the design and cryo-EM structural analysis of self-assembling α-helical nanotubes which can adopt one of two supramolecular architectures, Form I or Form II, based on precise adjustment of the peptide sequence[7]. Both Form I and Form II nanotubes are composed of α-helical stacks which self-assemble through non-covalent lateral interactions to form either monolayered or bilayered nanotubes. Form I nanotubes are characterized by cross α-helical linkages between a critical arginine clasp motif on the side of each protomer forming perpendicular hydrogen bonding networks with the C-terminal ends of adjacent protofilaments. The edge-to-side interactions of α-sheets generates high aspect-ratio single-walled nanotubes. The arginine clasp is used to describe the placement of an (RxxxR) pair of arginine residues arranged *i, i+4* which creates a conserved ipsilateral association domain. Because the clasp motif is the primary structural determinant of the resulting supramolecular assembly, modifying the length of the surrounding helix has a direct and predictable effect on the diameter and symmetry of the resulting nanotubes.

Form II peptides do not contain an arginine clasp, and therefore individual α-helices associate laterally to form a dimeric asymmetric unit through hydrophobic interactions which interact end-to-end via hydrogen bonding to form oblique cylindrical protofilaments which also associate laterally to form a bilayered nanotube. Interestingly, the mutation of the arginine clasp from *i, i+4* (RxxxR) to *i, i+3* (RxxR) converts Form I peptides to Form II, despite retaining an

ipsilateral pair of arginine residues, albeit at a different angular and axial displacement.

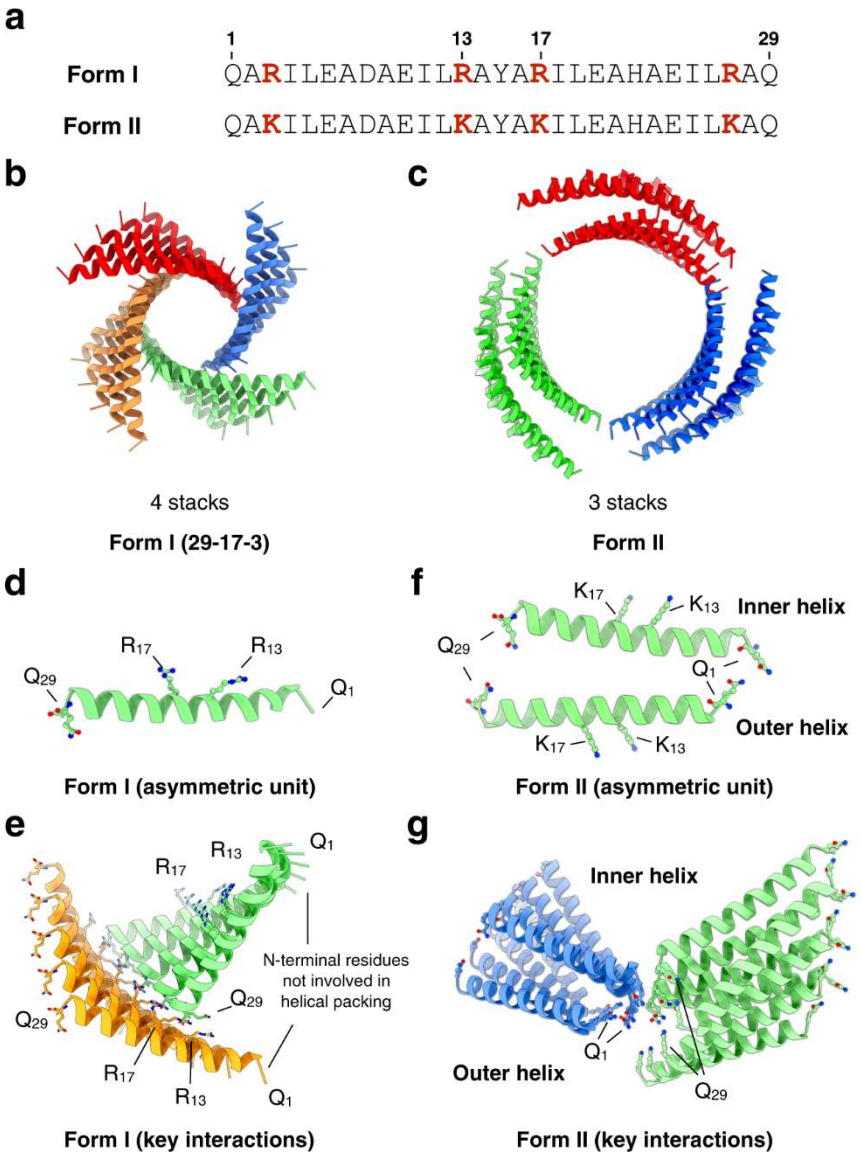

Figure 2. Figures taken from a recent publication in Nature Comm. by Gnewou et al[7]. Sequences of representative Form I and Form II peptides with key mutations highlighted **(a)**. Mutation of arginine to lysine drives a major conformational change in the resulting supramolecular structure. Structures of Form I **(b)** and Form II **(c)** peptides solved using Cryo-EM Asymmetric unit of Form I **(d)** and Form II **(f)** peptides, Form II peptides dimerize laterally. Key interactions mediating the self-assembly of protofilaments in Form I **(e)** and Form II **(g)**

With the knowledge that the polyproline-II-loop-α-helix fold motif was so robust and that the Form I and Form II peptides self-assembled so readily, we hypothesized that decoration of a self-assembling α-helix with a polyproline helix could produce a self-assembling miniprotein with convergent architectural principles. To test this claim, we designed and synthesized two peptide sequences, PPR and PPK as well as a control sequence, 21-16-2, isolating the α-helical region without a polyproline-II-helix or loop.

Peptide	Sequence and Helical Register *321321321321* loop *efgabc defgabc defgabcdefgabcdefg*
21-16-2	Ac - PEKLAA **Y**AEILA**R** **Y**A**R**ILAE**Y** - NH2
PP(R)	Ac - PP**R**EP**R**EP GDNAT PEKLAA **Y**AEILA**R** **Y**A**R**ILAE**Y** - NH2
PP(K)	Ac - PP**K**EP**K**EP GDNAT PEKLAA **Y**AEILA**R** **Y**A**R**ILAE**Y** - NH2
PPα	Ac - PPTKPTKP GDNAT PEKLAK **Y**QADLA**K** **Y**Q**K**DLAD**Y** - NH2
15-10-3 (Form I)	Ac - QAEIL**R**A YA**R**ILEAQ - NH2
29-20-2 (Form II)	Ac - QAE ILEADA**R** IL**R**AYEILKAHAEILKAQ - NH2

Table 1. Comparison of relevant sequences with a helical register for the polyproline helix and the α-helical heptad. Differences between PP(R) and PP(K) are highlighted in green. Tyrosine residues are transposed from PPα to a Form I scaffold, but the placement of charged residues at the *c* and *f* positions is retained.

PPR and PPK were designed using a (PPxxPxxP GDNAT) sequence motif derived from extensive screening by the Woolfson group[5,6] to generate the polyproline helix and loop in their PPα series. Although the Woolfson group chose to design positive (PPKKPKKP) and negatively

(PPEEPEEP) charged polyproline helices to pair with oppositely charged α-helices, we chose to use an amphiphilic sequence (PPXEPXEP, where X is either R or K) because the self-assembling α-helix sequence we adapted is likewise amphiphilic. The helical segment was adapted from 15-10-3, the shortest Form I peptide, but with the arginine clasp replaced by an (RxxR) motif to match the charged residues on PPα. 29-20-2 is a Form II peptide containing an analogous (RxxR) motif at the *c* and *f* positions of the heptad.

Key sequence homologies between PPR, PPK, PPα, and 29-20-2 are shown in Table 1. Tyrosines are placed strategically at the *d* position of the α-helical heptad to establish interdigitation with the adjacent polyproline helix. The (RxxR) motif is positioned contralateral to the hydrophobic core at the *c* and *f* positions to permit lateral non-covalent interactions. Although 29-20-2 adopted a Form II configuration, it is feasible that the bulk of the polyproline-II-helix will hinder the formation of a dimeric asymmetric unit and will instead prefer a Form I type side-to-edge perpendicular association.

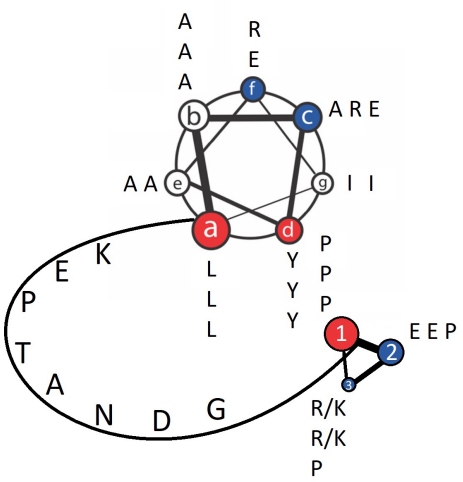

Figure 3. Helical wheel representation of proposed coiled-coil type packing between the two helical counterparts bridged by a loop region. Positions corresponding to the hydrophobic core

are colored red, positions containing residues with charged or hydrophilic sidechains are marked in blue.

Results and Discussion:

Peptide Synthesis and Assembly: PPR, PPK, and the control helix (21-16-2) were synthesized using microwave assisted solid-phase peptide synthesis. Peptides were purified using reversed-phase HPLC on a C-18 column followed by lyophilization to yield a white powder. The identity of each peptide was confirmed using MALDI-TOF mass spectrometry. Conditions for assembly were screened across multiple buffers to identify the optimal pH for self-assembly. Peptides were dissolved at 3mg/mL of aqueous buffer (10mM acetate pH 4.0, 10mM acetate pH 5.0, 10mM MES pH 6.0, 10mM MOPS pH 7.0, 10mM TAPS pH 8.0, 10mM CAPS pH 10.0) and allowed to assemble in ambient conditions at room temperature. Aliquots of each buffer condition were also taken and annealed directly after dissolving by rapidly heating in a thermocycler to 90°C for 30 minutes and cooling to 25°C at a rate of 0.2°C/minute.

Circular Dichroism (CD): Circular dichroism spectropolarimetry was used to investigate the various assembly conditions and to confirm the presence of secondary structural characteristics (Figure 4.).

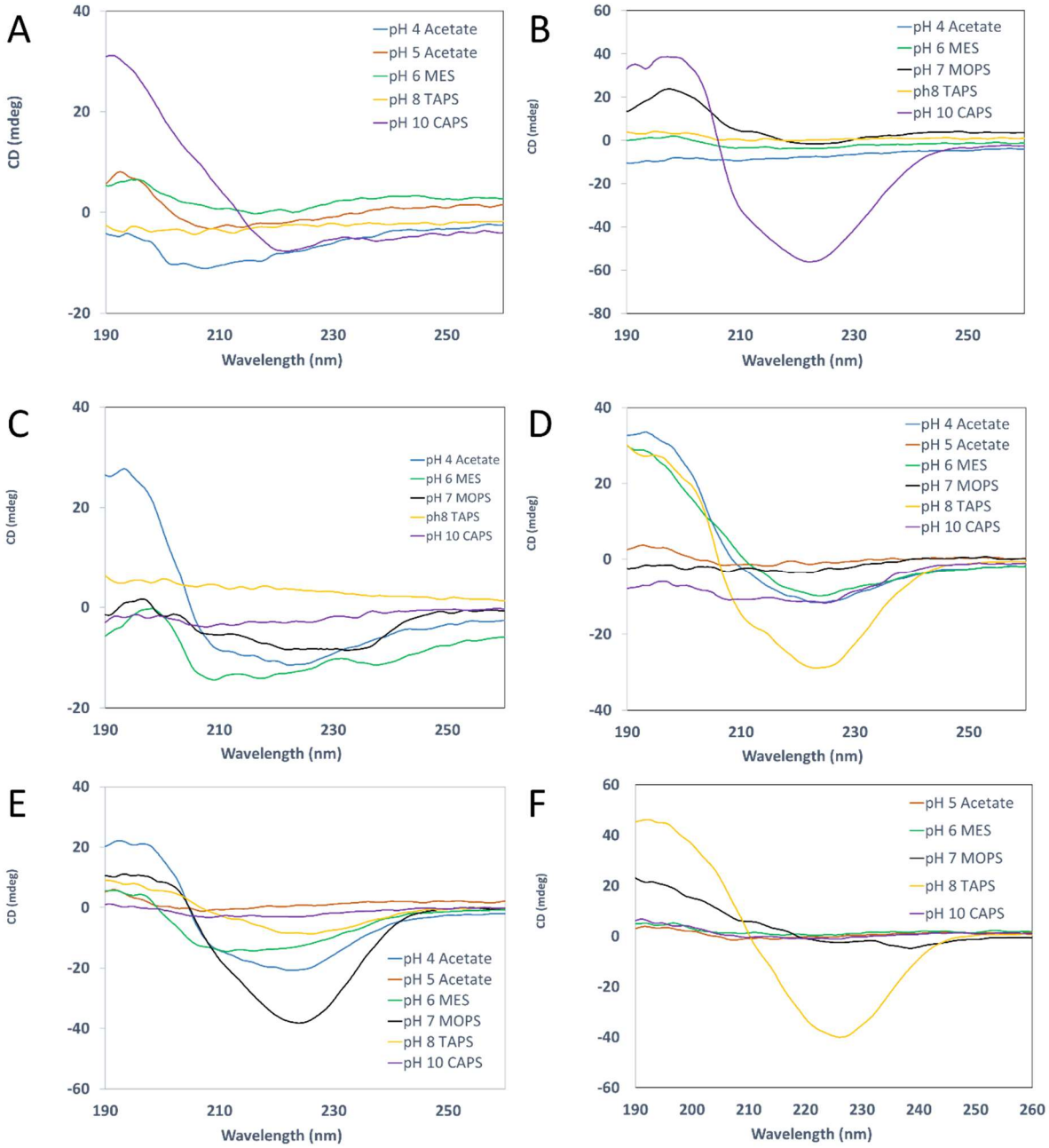

Figure 4. Peptides were assembled at a concentration of 3mg/mL in 10mM buffer, CD spectra are shown for 21-16-2 annealed **(a)** 21-16-2 unannealed **(b)** PPR annealed **(c)** PPR unannealed **(d)** PPK annealed **(e)** PPK unannealed **(f)**

Although positive cotton effects were generally observed across all the conditions investigated, a clearly resolved double minima particularly at 208nm was not easily discernible although this may in part be due to the interference of multiple secondary structures. Minima for a substituted polyproline-II-helix containing secondary amides occurs at 195nm with maxima at 212nm[8] which could account for lower fidelity and smoothing of the spectrum in areas where characteristics of α-helices normally appear. Right-handed secondary structures appear to recur, but the strength of secondary structure formation varies significantly with changes in the pH of assembly conditions.

The highest magnitude mean residue ellipticities (MRE) were measured in 10mM CAPS pH 10.0 for annealed and unannealed 21-16-2, 10mM Acetate pH 4.0 for unannealed PPR, 10mM TAPS pH 8.0 for annealed PPR, 10mM TAPS pH 8.0 for unannealed PPK, and 10mM MOPS pH 7.0 for annealed PPK.

Transmission Electron Microscopy (TEM): Transmission electron microscopy images were taken of samples that were allowed to assemble at room temperature for a month and negatively stained with 1% Uranyl Acetate (UA) solution. Unannealed samples assembled in 10mM Acetate, pH 4.0 buffer for a month were imaged first, showing a wide range of ordered structures. High aspect ratio filaments (~10nm width) without visible lumens were observed for 21-16-2. Grids with PPR showed a dense mesh of supramolecular structures, including large, flat

tapes of varying widths which could be seen forming into ribbons and tubes as well as structurally distinct strands of filaments. PPK contained primarily unassociated protein aggregates, but short fibrils and longer filaments did emerge.

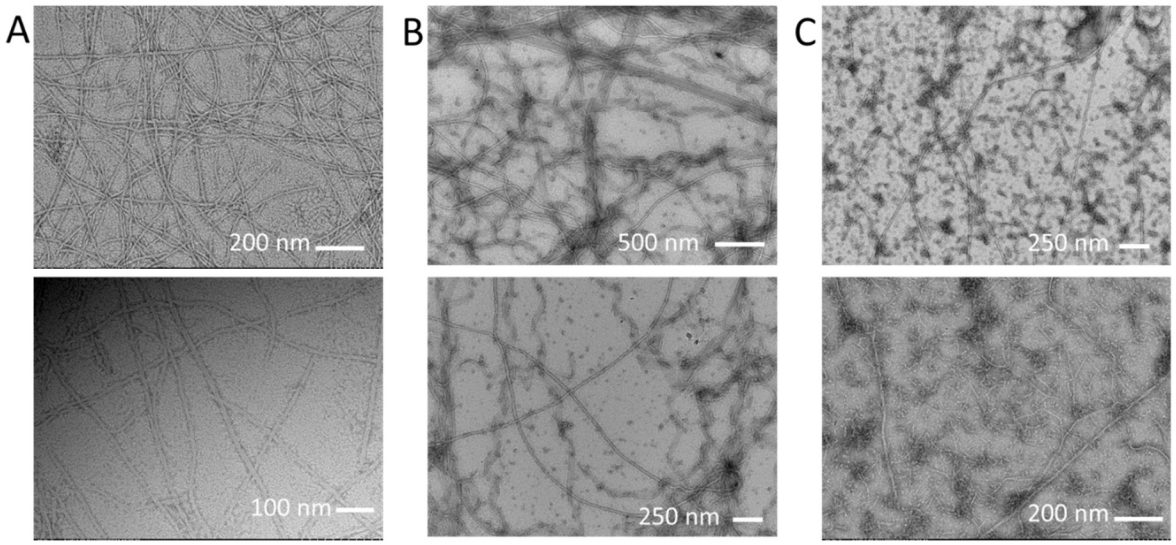

Figure 5. Representative TEM images taken of peptides assembled under ambient conditions in 10mM pH4.0 acetate stained with 1% UA . 21-16-2 **(a)** PPR **(b)** PPK **(c)**. Scale bars are shown in white.

Unfortunately, the results from the other assembly conditions could not be collected due to an extended campus closure which would last until the subsequent year, at which time all of the assembled samples had dried up or been disposed. The remaining powder was assembled more than 2 years later in 10mM acetate pH 4.0 buffer in an effort to replicate the data, but the efforts were in vain. It's highly likely that the protein had degraded significantly, as an ESI mass spectrometry reading of the stored powder showed no trace of the expected mass.

Conclusion:

Although there was clear evidence of higher order supramolecular assembly of PPR, the irregularity of the structures and the simultaneous presence of multiple nano-architectures would have made cryo-EM structure elucidation impossible for the conditions investigated. Based on the CD data, it is possible that the assembly of PPR or PPK could have converged on a single thermodynamically stable structure at a higher pH or after annealing, but this is pure speculation, and the existence of secondary structures does not necessitate the formation of pure tertiary or quaternary organizations. This project was successful as a proof-of-concept unification of distinct peptide and protein folding paradigms, and further study of miniprotein-peptide conjugates could yield productive insights into which paradigms dominate the resulting structural and material properties of the resulting folded peptide. The self-assembly of miniprotein oligomers also offers insight into the potential of larger globular proteins to misfold and self-assemble into aggregates while retaining much of their globular structure. The incorporation of self-assembling domains in naturally occurring proteins and peptides has been documented extensively for amyloid fibril formation[9], but this project explores an example of ordered aggregation of protein-like molecules by an α-helical regime.

Materials and Methods:

Materials: All chemical reagents were purchased from Fisher Scientific, Inc. (Pittsburgh, PA), Anaspec, Inc (Fremont, CA) or Sigma-Aldrich Chemical Co. (St. Louis, MO) unless otherwise specified and used without further purification.

Peptide Synthesis and Purification: Peptides were synthesized on a 5 μmol scale using a CEM Liberty Blue microwave-assisted solid phase peptide synthesizer. Fmoc-protected amino acids were attached to a PAL-PEG-PS resin from Applied Biosystems (Foster City, CA) to produce a C-terminal amide. Standard Fmoc protection/deprotection chemistry was used with coupling cycles based on HBTU/Oxima activation protocols and base induced deprotection (20% piperidine in N, N-dimethylformamide with 0.1 M hydroxybenzotriazole) of Fmoc protecting group. All arginine groups were double coupled. Acetylation of the N-terminal (20% acetic anhydride in N, N-dimethylformamide) occurred with the final deprotection cycle.

After synthesis, the coupled resin was washed with DMF and transferred to a Buchner funnel to be washed with acetone and dried in vacuo. The crude peptide was subjected to a cleavage protocol to separate it from the support resin using a solution of 92.5% trifluoroacetic acid, 2.5% triisopropylsilane, 2.5% 3,6-Dioxa-1,8-octanedithiol, and 2.5% water. The cleavage solution was filtered and precipitated by centrifuge with cold diethyl ether (4ºC).

Peptides were purified with a Shimadzu LC-20AP preparatory reverse-phase HPLC with C18 column across a linear gradient of water/acetonitrile with 0.1% trifluoroacetic acid. Product identity was confirmed using matrix-assisted laser desorption/ionization time of flight (MALDI-TOF) mass spectrometry in a α-Cyano-4-hydroxycinnamic acid (CHCA) matrix. Product peaks were collected and dried in vacuo and lyophilized to yield a white powder.

Circular Dichroism: CD measurements were taken on a Jasco J-1500 CD Spectropolarimeter using a 0.20 mm quartz cuvette (Hellma USA Inc, Plainveiw, NY). Signals were measured three times consecutively, averaged, and corrected with a blank spectrum of the corresponding buffer. Spectra were taken with a scan rate of100nm/min from 190-260nm with a bandwidth of 2nm and data pitch of 0.2nm.

Negative Stain and TEM analysis: TEM grids were prepared with assembled samples of peptide at 3mg/mL concentration. 4µL of each sample were deposited onto 200-mesh carbon-coated copper grid (Electron Microscopy Services, Hatfield, PA) and allowed to incubate for 90 seconds. Excess liquid was wicked away and 4µL of 1% Uranyl Acetate solution was deposited onto the grid surface and incubated for 90 seconds. Remaining moisture was wicked away, and electron micrograph images were collected on a Hitachi HT-7700 transmission electron microscope. The microscope is equipped with a tungsten filament, an AMT CCD camera, and operates at an accelerating voltage of 80kV.

References:

1. RCSB Protein Data Bank: powerful new tools for exploring 3D structures of biological macromolecules for basic and applied research and education in fundamental biology, biomedicine, biotechnology, bioengineering and energy sciences (2021) Nucleic Acids Research 49: D437–D451 doi: 10.1093/nar/gkaa1038
2. Gellman, S. H.; Woolfson, D. N. Mini-Proteins Trp the Light Fantastic. Nat. Struct. Biol. 2002, 9, 408−410.
3. Blundell TL, Pitts JE, Tickle IJ, Wood SP, Wu CW. X-ray analysis (1. 4-A resolution) of avian pancreatic polypeptide: Small globular protein hormone. Proc Natl Acad Sci U S A. 1981 Jul;78(7):4175-9. doi: 10.1073/pnas.78.7.4175. PMID: 16593056; PMCID: PMC319751.
4. Baker EG, Bartlett GJ, Porter Goff KL, Woolfson DN. Miniprotein Design: Past, Present, and Prospects. Acc Chem Res. 2017 Sep 19;50(9):2085-2092. doi: 10.1021/acs.accounts.7b00186. Epub 2017 Aug 23. PMID: 28832117.
5. Baker, E., Williams, C., Hudson, K. et al. Engineering protein stability with atomic precision in a monomeric miniprotein. Nat Chem Biol 13, 764–770 (2017). https://doi.org/10.1038/nchembio.2380
6. Stabilizing and Understanding a Miniprotein by Rational Redesign Kathryn L. Porter Goff, Debbie Nicol, Christopher Williams, Matthew P. Crump, Francis Zieleniewski, Jennifer L. Samphire, Emily G. Baker, and Derek N. Woolfson, Biochemistry 2019 58 (28), 3060-3064 DOI: 10.1021/acs.biochem.9b00067
7. Wang, F., Gnewou, O., Modlin, C. et al. Structural analysis of cross α-helical nanotubes provides insight into the designability of filamentous peptide nanomaterials. Nat Commun 12, 407 (2021). https://doi.org/10.1038/s41467-020-20689-w

8. Circular Dichroism Spectrum of Peptides in the Poly(Pro)II Conformation, Robert W. Woody, Journal of the American Chemical Society 2009 131 (23), 8234-8245 DOI: 10.1021/ja901218m
9. Dobson, C. Protein folding and misfolding. Nature 426, 884–890 (2003). https://doi.org/10.1038/nature02261

Chapter 2: Characterization of Amphiphilic β-sheet Analogues

Introduction and Design:

The hierarchical assembly of amphiphilic β-sheet forming peptides inspired by naturally occurring sequence motifs found in fibrous proteins is one of the most robust self-assembly archetypes available[1,6,7]. Self-assembly of β-sheet filaments occurs readily when a sequence is composed of alternating hydrophobic and hydrophilic residues (XZXZ… where X is a polar, hydrophilic residue and Z is a nonpolar, hydrophobic residue or vice versa), a structural motif first proposed by Pauling and Corey in their study of silk fibroin[2]. Segregation of hydrophobic and hydrophilic residues onto opposite faces of β-sheet secondary structures promotes lamination of sheets to form cross-β bilayers which associate through non-covalent sidechain interactions to form amyloid fibrils (Figure 6.).

The processes leading to the formation of amyloid fibrils is of particular interest due to the role of amyloid in many degenerative diseases including Alzheimer's, Parkinson's, Type II Diabetes, and various prion diseases[1,7]. Designer peptides utilizing this alternating structural motif assemble rapidly and show robust environment dependent assembly while retaining dimensional and stereochemical properties of naturally occurring amyloid fibers[1]. Synthetic and natural polypeptides with virtually no sequence homology show convergence into a cross-β architecture, particularly under denaturing conditions[7,8]. The ubiquity of amyloid formation is thus a significant subject of scientific inquiry and investigation.

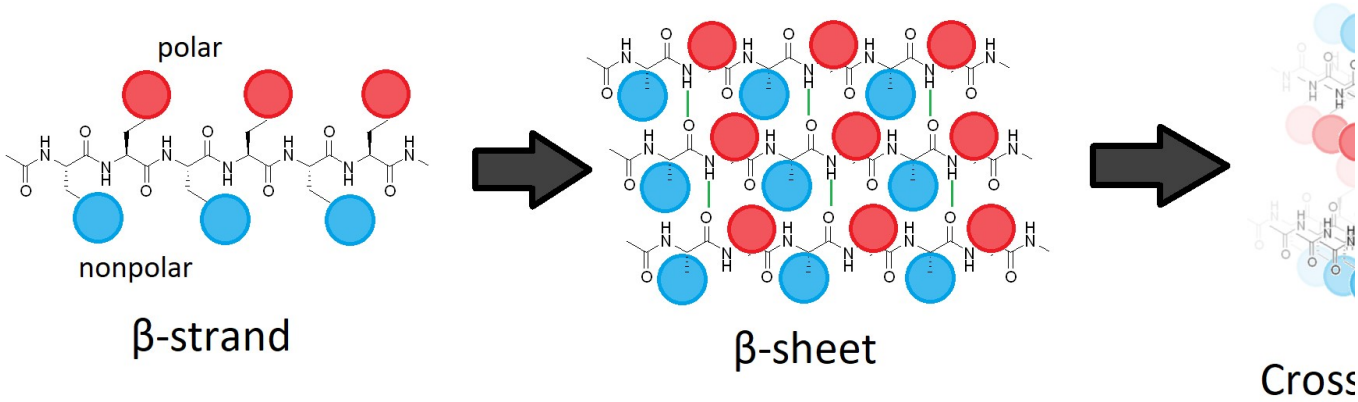

Figure 6. General scheme for the self-assembly of amphiphilic β-strands with alternating polar and nonpolar sidechains into β-sheets through backbone binding and formation of a β-sheet bilayer driven by lamination of hydrophobic residues to produce amyloid fibrils[1].

The short oligopeptide KFE8 (Ac-$(FKFE)_2$-NH_2) is a well-studied amphiphilic β-strand that readily self-assembles into β-sheet fibrils which display characteristics of amyloid fibers[1,3-5,11,12,15]. KFE8 assemblies form hydrogels when the ionic strength or pH of the assembly buffer meet certain thresholds and have demonstrated efficacy in transporting small hydrophobic molecules across cellular membranes[1,16,17]. KFE8 has a well understood folding pathway involving the formation of an intermediary helical ribbon morphology that coalesces into stable nanotubes[4,12]. The Conticello group has utilized high resolution cryo-electron microscopy to conduct near-atomic structural analysis of KFE8 and revealed condition dependent structural plasticity of the supramolecular helical ribbons and tapes that KFE8 forms. Annealed KFE8 assembles into two stable morphologies of double-walled nanotubes possessing either 4-fold or 5-fold point symmetry with corresponding widths of 7.5nm and 8.5nm respectively[12]. Notably, this marks the first instance of a designed β-sheet assembly structure being solved by cryo-EM,

which provides unique insight into long-range supramolecular structure that traditional solid state NMR techniques cannot[10,13].

As a biomaterial with multiple potential applications as an injectable hydrogel[16], a drug delivery system[17], or a minimalist model for the formation of amyloid[4], KFE8 is a remarkable example of *de novo* peptide design. Having solved the structures of KFE8, we wanted to continue to explore and tune the properties of similar β-sheet structures. Previous research has shown the effects of alterations to the hydrophobicity of KFE8, with significant changes in the self-assembly behavior and properties of peptides when phenylalanines were substituted with aliphatic residues with higher hydrophobicity indices[15,16]. We proposed three direct analogues of KFE8 to characterize and test the physiochemical and self-assembly properties of KFE8 analogues with increased hydrophilicity (Table 2).

Peptide	Sequence
KFE8	Ac – FKFEFKFE – NH2
RFE8	Ac – F**R**FEF**R**FE – NH2
KFE7	Ac – KFEFKFE – NH2
KFE9	Ac – KFEF**Q**FKFE – NH2

Table 2. Table of relevant peptide sequences. Mutations of lysine to arginine are bolded in RFE8. KFE7 has an abridged sequence with the N-terminal phenylalanine subtracted from KFE8. KFE9 has a hydrophilic glutamine residue inserted into the center of the sequence and the order of the first 4 residues are rearranged to maintain polar sequence patterning.

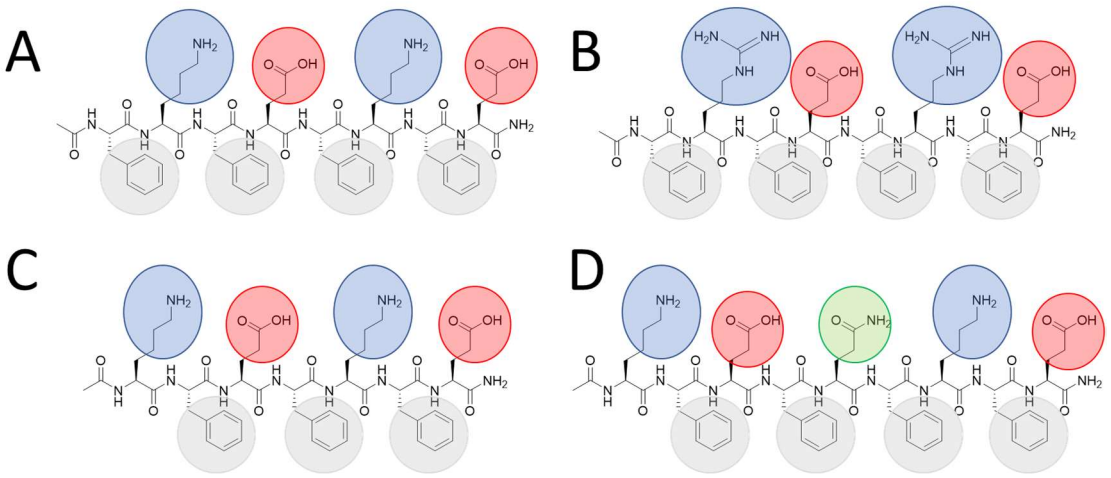

Figure 7. Molecular design basis of KFE8 **(A)**, RFE8 **(B)**, KFE7 **(C)**, and KFE9 **(D)**. Charged residues (Blue (+) and Red (-)) are alternated to establish potential salt bridges which stabilize and direct self-assembly[12,18] while remaining on the same face of the resulting β-sheet. Hydrophobic residues are likewise oriented along the same face of the β-strands. Introduction of the hydrophilic, but uncharged glutamine in KFE9 increases hydrophilicity without interfering with ionic salt-bridges.

RFE8 (Ac-(FRFE)$_2$-NH$_2$) substitutes lysine residues of KFE8 with arginine residues to ascertain if altering the hydrophilic character of the peptide sequence via mutation influences self-assembly. Although RFE8 remains amphiphilic and has the same sequence length and pattern of alternating hydrophobic and hydrophilic residues as KFE8, the intrinsic hydrophobicity of Arg is distinct from Lys, with Arg being more hydrophilic at lower pH and more hydrophobic as pH approaches neutral[11]. One may also recall that lysine to arginine mutations of Form II peptides from the previous chapter induced significant change to the resulting morphology of assemblies.

KFE7 (Ac-KFEFKFE-NH_2) has a deletion of the N-terminal phenylalanine from KFE8 and KFE9 (Ac-KFEFQFKFE-NH_2) contains a hydrophilic but uncharged glutamine inserted into the center of the nonapeptide sequence. The first FKFE motif is mutated to KFEF to maintain the pattern of alternating polar and nonpolar residues. These analogues were designed to explore the influence of introducing asymmetry between the hydrophobic and hydrophilic faces of the individual β-strands. The amphiphilicity of KFE7 and KFE9 is retained from KFE8, but the overall hydrophilicity of the analogues is increased. Both analogues have larger hydrophilic surfaces than their corresponding hydrophobic surfaces whether it is through deletion or through insertion of a nonpolar or polar residue.

Results and Discussion:

Peptide Assembly: Peptides were purchased from GenScript USA Inc (Piscataway, NJ) and used without further purification. Peptides were initially assembled in 10mM acetate buffer at pH 4.0 at a concentration of 3mg/mL by dissolving measured quantities of the powdered peptide in a 1:1 ratio of deionized water and 20mM acetate buffer and vortexing until particulates disappeared. Assemblies were titrated using dilute sodium hydroxide and hydrochloric acid to achieve a pH of 4.0. These conditions were replicated from prior experiments with KFE8 which were optimized to slow the rate of assembly and reduce irreversible aggregation[3,4,12]. Aliquots of each peptide were taken directly after assembly and annealed by heating in a thermocycler to 90°C for 30 minutes and cooling to 25°C at a rate of 0.2°C/minute. The remainder of the assemblies were sealed and left under ambient conditions.

Peptides were later assembled in 10mM acetate titrated to pH 5.0, 10 mM MES titrated to pH 6.0, 10mM MOPS titrated to pH 7.0, and 10mM TAPS titrated to pH 8.0 to discern any differences in assembly at higher pH conditions. The same protocol for assembly was used,

however these assemblies were not annealed, and were only assembled at ambient temperatures. Assemblies remained stable in solution and there was no indication of crystallization or precipitation even after 6 weeks, however high pH (7.0 and 8.0) assemblies of KFE9 become noticeably viscous after 1 week.

Circular Dichroism: CD spectra of the peptides initially assembled in 10mM acetate at pH 4.0 were taken at multiple timepoints to observe the formation of secondary structures over time. Samples were taken from the ambient condition assemblies 1 hour after assembly and 72 hours after assembly. Because the annealing process takes 72 hours to reach room temperature, CD measurements of the annealed peptides were taken directly after peptides finished annealing at the same time as the ambient peptides. It should be noted that although circular dichroism analyses of α-helical peptides and proteins tends to exhibit high spectral uniformity, β-structured proteins display massive spectral diversity which makes characterization and identification of β-sheet content less visually obvious. Algorithms such as the Beta Structure Selection (BeStSel) method can be used to accurately determine secondary structure content[9].

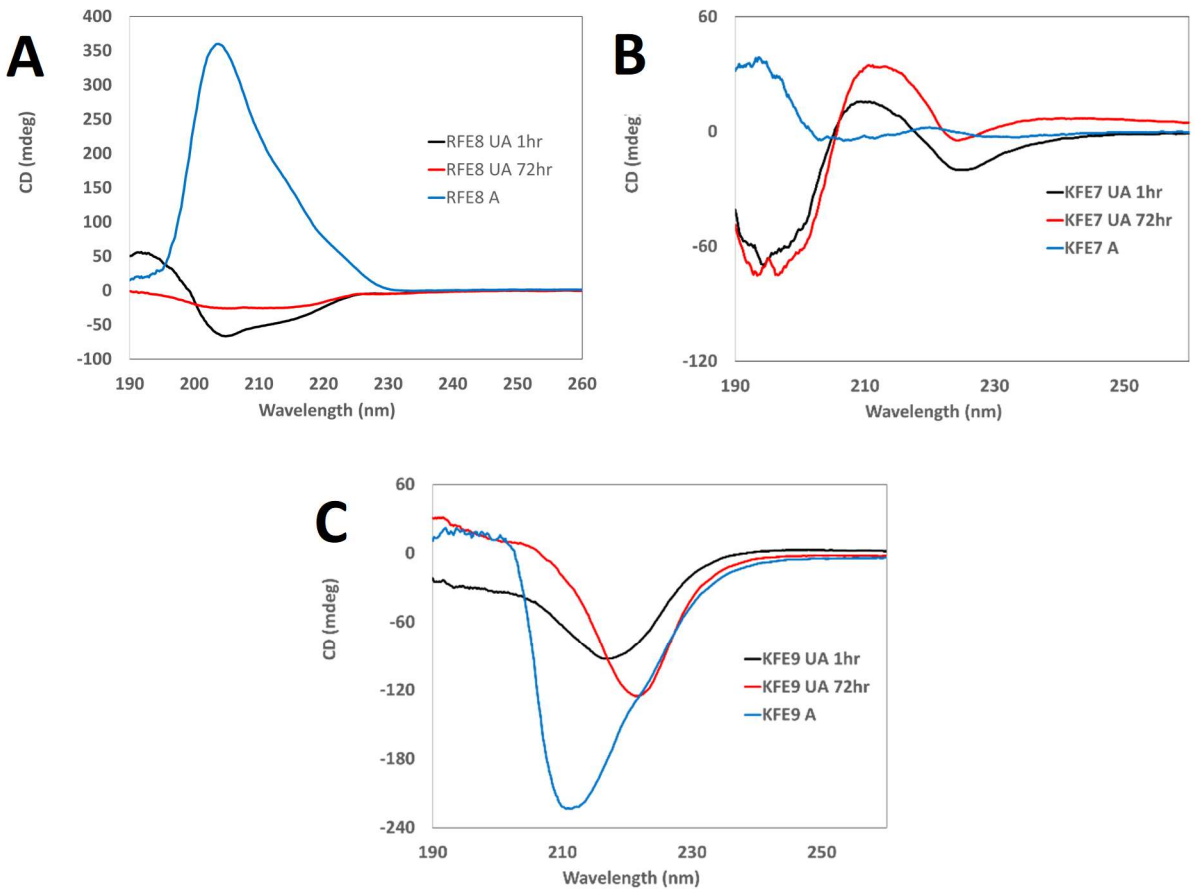

Figure 8. Overlaid CD spectra of RFE8 (A), KFE7 (B), and KFE9 (C) assembled in 10mM pH4 acetate at 3mg/mL after 1 hour at room temperature (black), after 72 hours at room temperature (red), and after annealing (blue).

RFE8 showed a potentially α-helical trace after 1 hour, with a distinct maximum at 192nm, a minimum at 206nm and a shoulder at 216nm, but this signal devolved after 72 hours into a significantly weaker signal showing a possible double minimum at 206nm and 213nm. Given the negative Cotton effect that emerges, it is still fair to assume that β-sheet character has developed. The annealed sample displayed an entirely positive Cotton effect, which implies

reversal in the helical sense of secondary structures observed in the unannealed samples. This is possibly due to the formation of parallel beta sheets as opposed to antiparallel but could also be indicative of a right-handed screw axis in the interactions of chromophores in the annealed RFE8 as opposed to a left-handed screw axis of interaction in the unannealed. The measured ellipticity is also much stronger in the annealed samples, implying a higher degree of structural conformity and order.

The CD spectra of KFE7 were extremely weak and showed a significant amount of noise at both time points and after annealing. The observed negative Cotton effect and distinct lack of a double minimum implies some formation of β-sheets in the ambient samples, and there is once again an inversion of the Cotton effect for the annealed sample however the noisiness of the measurements suggests that most of the sample remains disordered.

CD measurements of KFE9 show a distinctive negative Cotton effect that is seen across all conditions, including the annealed. The large single minimum fluctuates from 217nm to 221nm between hour 1 and hour 72 and is measured at 211nm in the annealed sample. The magnitude of the measured ellipticity increased marginally from hour 1 to hour 72 and was strongest in the annealed sample. The pattern is strongly indicative of homogenous β-sheet formation.

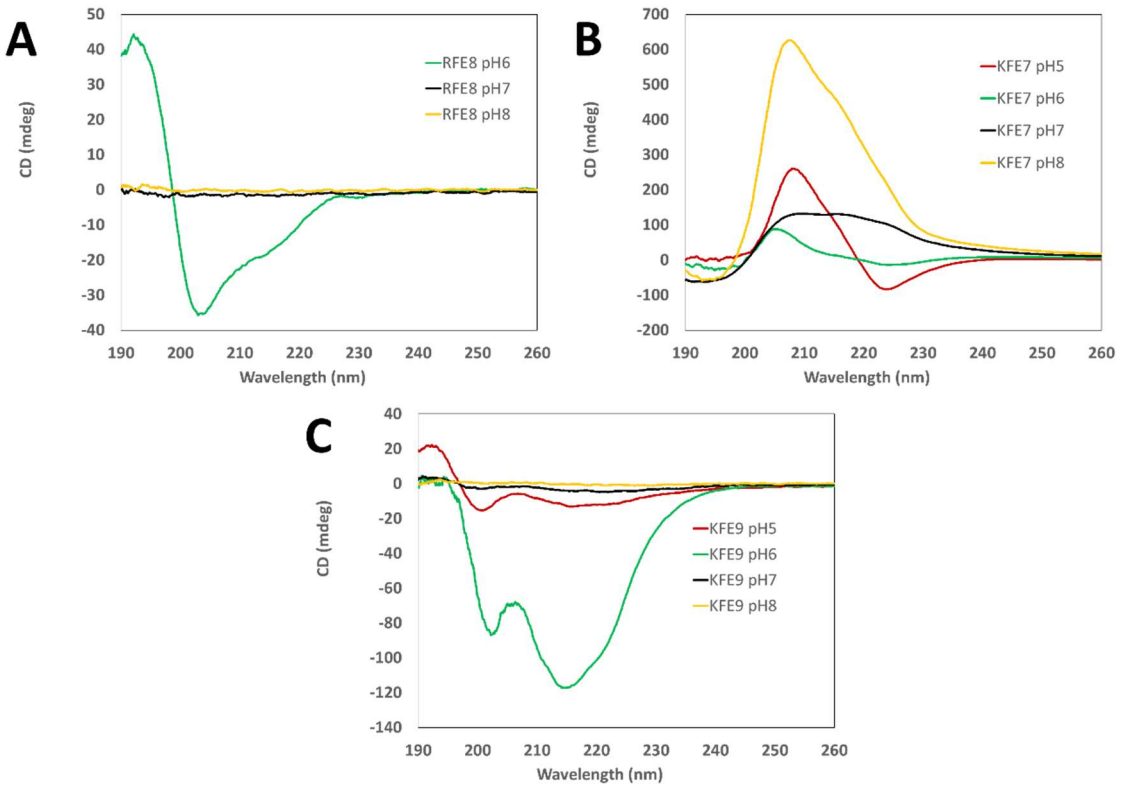

Figure 9. Overlaid CD spectra of RFE8 (A), KFE7 (B), and KFE9 (C) assembled at 3mg/mL in 10mM pH5.0 acetate, 10mM pH6.0 MES, 10mM pH7.0 MOPS, and 10mM pH8.0 TAPS at room temperature for 6 hours.

Circular dichroism was also used to characterize the assembly of peptides in higher pH buffers. Spectra were taken from samples that were allowed to assemble in ambient conditions for 6 hours. RFE8 displayed secondary structure formation in 10mM MES buffer at pH6.0, corresponding closely to the spectra measured in acetate buffer after 1 hour, with the same maximum at 193nm, a minimum at 203nm, and a shoulder at 214nm. Assemblies in higher pH buffers (pH7.0 MOPS, pH8.0 HEPES) do not exhibit any measurable secondary structure

content. The data from RFE8 assembled in 10mM acetate titrated to pH5.0 are not included because the amount of reagent available was insufficient for the collection of meaningful data.

KFE7 shows indications of ordered secondary structure formation with traces that are shaped roughly congruously, with the highest measured ellipticity in pH8.0 TAPS buffer. A characteristic single peak at ~206-210nm was observed in all conditions, with general indication of β-sheet formation across the board. KFE9 displays a crude, but well-defined double minimum at ~201nm and 215nm in pH5.0 acetate and pH6.0 MOPS. The CD signal degenerates significantly at pH7.0 and pH8.0. The CD taken from the pH5.0 buffer appears to be α-helical in character, with a positive cotton effect including a maximum at 191nm, and two local minima at 201nm and 215nm, although this pattern isn't as defined in other assemblies. The lack of a positive maximum in the CD spectrum of KFE9 assembled at pH6.0 points away from α-helical structural content, although there is still a double minimum at 202 nm and 214nm. BeStSel analysis suggests that the signal is representative of antiparallel β-sheet character[9].

Transmission Electron Microscopy: The initial assemblies of RFE8, KFE7, and KFE9 in pH4.0 acetate were examined by TEM after 1 week and after 6 weeks of incubation. Samples were negatively stained using 1% Uranyl Acetate for the 1-week samples, but difficulty acquiring images with appropriate contrast prompted the use of 1% Phosphotungstic acid (PTA) stain for the remainder of the project.

RFE8 (pH4): Unannealed RFE8 assembled in pH4.0 acetate formed two distinct morphologies: helical ribbons that are visually similar to those observed in newly assembled unannealed KFE8[4,12] as well as straight filaments with an average diameter of 11.25 nm and clearly defined lumens that indicate a hollow central tube. The measured width of the nanotubes observed for RFE8 are higher than those measured in KFE8[12]. Many instances of helical ribbons

converging into nanotubes could be observed, suggesting that much like KFE8, the helical ribbons are intermediates for the formation of nanotubes. Annealed RFE8 samples display nanotubes with an average width of 11.44 nm, as well as wider filaments or tapes with an average width of 17.29 nm that can be identified by their lack of visible lumen. It is difficult to confirm if the wider filaments are of a different supramolecular architecture than the tubes with lumens, as it is possible that they are just flattened or otherwise distorted nanotubes that are shaped such that stain was unable to penetrate into an inner cavity. No traces of helical ribbons were observed.

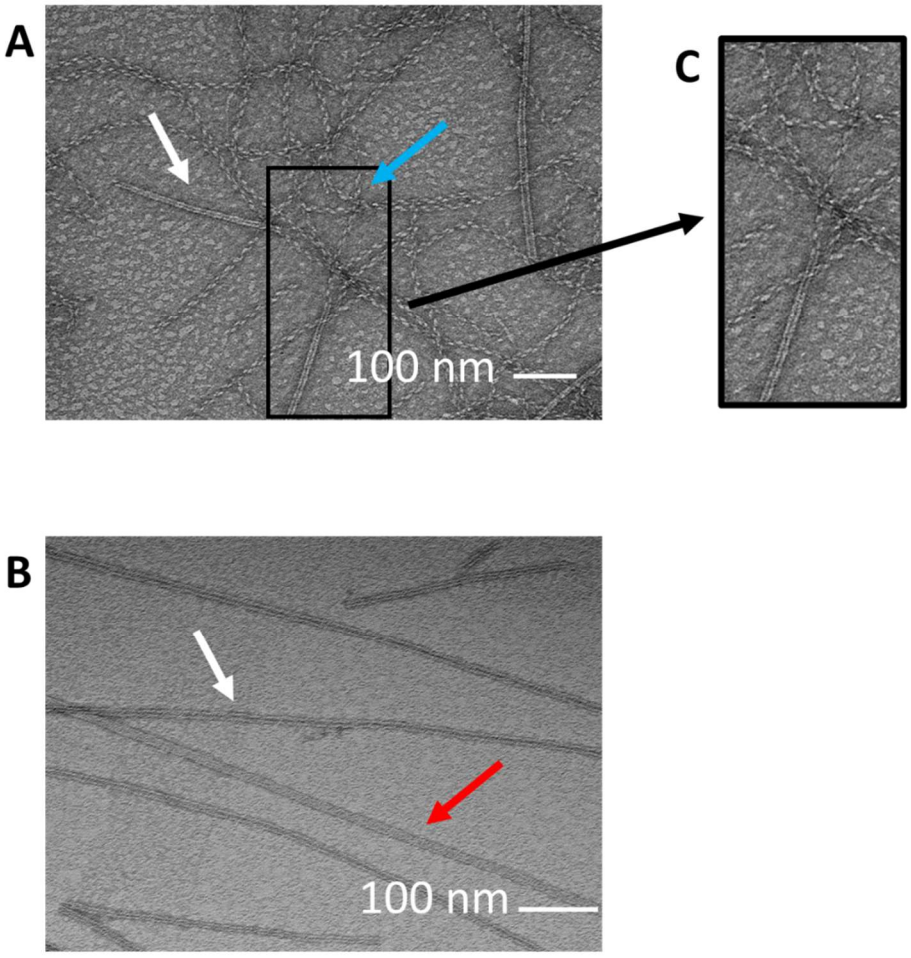

Figure 10. Representative TEM images of RFE8 assembled in 10 mM pH4.0 acetate and stained with 1% UA exhibits various supramolecular morphologies depending on assembly conditions. Unannealed RFE8 incubated for 1 week (A) shows helical ribbons (blue arrow) and straight tubular filaments (white arrow). Annealed RFE8 (B) developed straight tubular filaments corresponding to filaments observed in the unannealed sample (white arrow) and as well as wider, flatter filaments (red arrow).

After 6 weeks of assembly, helical ribbons remained present in the images taken of unannealed RFE8, although at a slightly lower proportion than after 1 week of assembly. Unlike the KFE8, where the population of helical ribbons decreased significantly after 2 weeks of incubation[12], RFE8 either has a significantly slower rate of assembly, or approaches a steady state equilibrium with a higher rate of exchange between the helical ribbon and tubular filament morphologies.

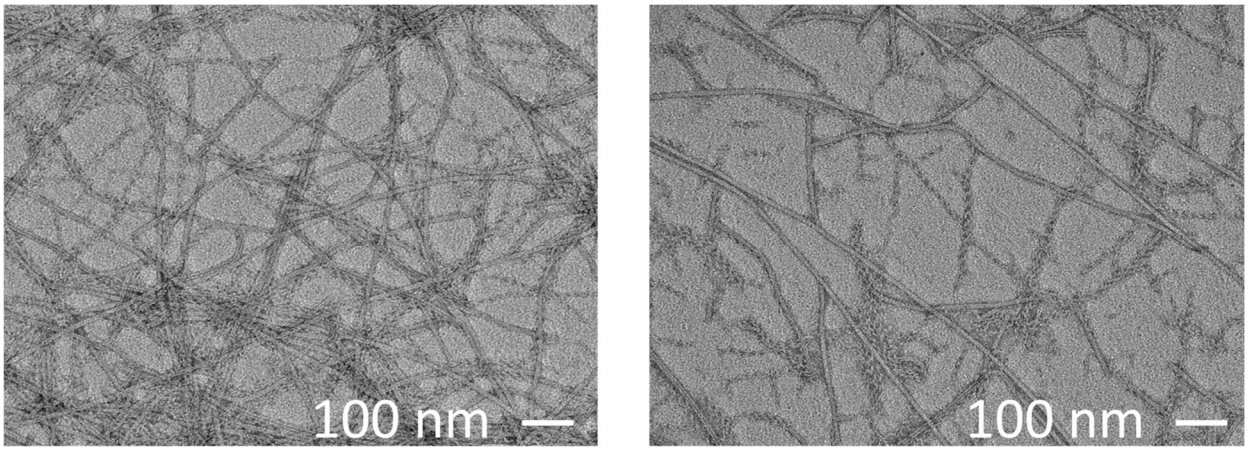

Figure 11. Representative TEM images of RFE8 allowed to assemble for 6 weeks in pH4 acetate at room temperature and stained with 1% PTA. A heterogenous population of helical ribbons and straight filaments can be observed evenly dispersed throughout.

KFE7 (pH4): TEM imaging of unannealed KFE7 after 1 week was largely inconclusive. Sparse populations of fibrils could be observed, but there was very little uniformity in their appearance, length, or aspect ratio. Annealed KFE7 formed a dense mesh of fibrils, fibers and aggregated or unassembled peptide that was also difficult to interpret or clearly resolve. Flexible loops of fibrillar quality were observed throughout the grid, but the widths and lengths of the fibrils is impossible to determine.

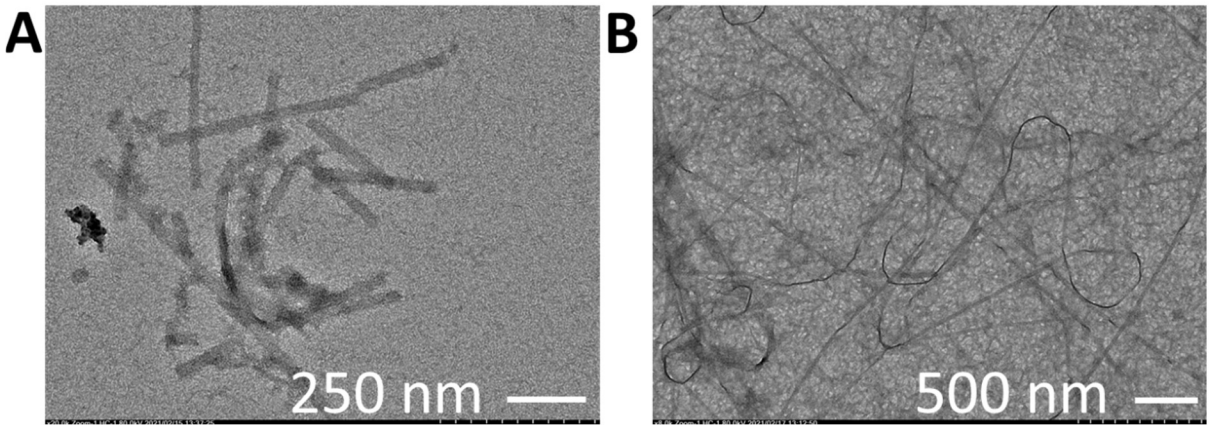

Figure 13. Representative TEM images of KFE7 assembled in 10mM pH4.0 acetate at 3mg/mL under ambient conditions for 1 week (A) and after annealing (B), samples are stained with 1% UA. Little to no higher order structure or assembly was observed in the ambient sample, a mesh of thin filaments and aggregated or unassembled protein was seen throughout the annealed sample.

After 6 weeks of assembly in pH4.0 acetate, the unannealed KFE7 stained with 1% PTA showed a mixed population of filaments of varying length and width, including long flat sheets and thin twisted strands that showed a tendency to form tangled braids. We hypothesize that the thinner filaments can associate laterally to form larger sheets. Although some twisting and folding of sheets was observed, there was no indication of any tubular morphologies that emerged.

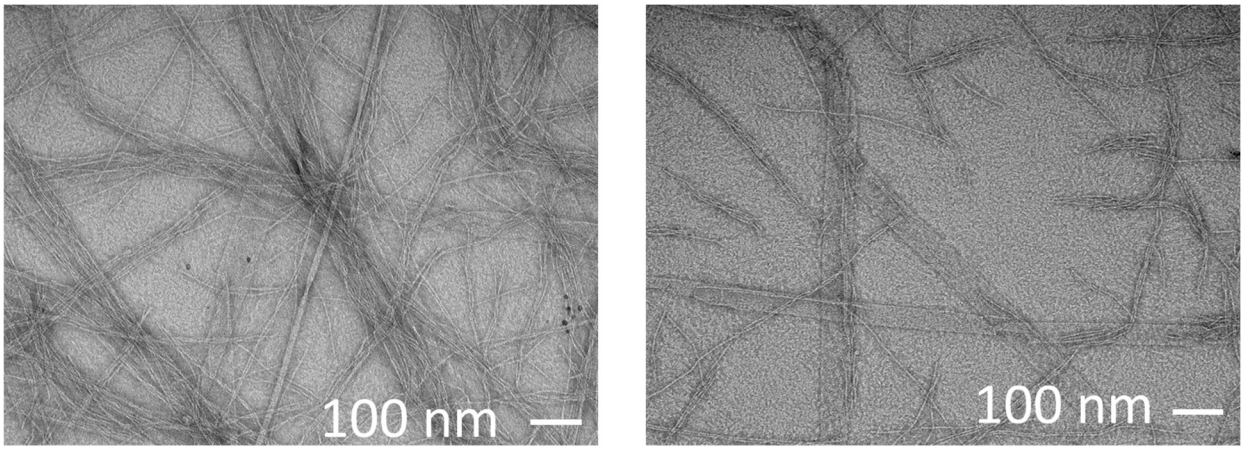

Figure 14. Representative TEM images of KFE7 allowed to assemble for 6 weeks in pH4 acetate at room temperature and stained with 1% PTA. Wide, flat filaments and sheets of highly variable width are observed interspersed with many thinner filaments and fibrils.

KFE9 (pH4): Unannealed KFE9 after 1 week was largely composed of dense aggregates with some fibrous character. Many small fibrils are seen sticking together in small clumps, but longer filaments were not observed at all. Annealed KFE9 exhibited longer fibrils, including several instances of filaments with twisted strands.

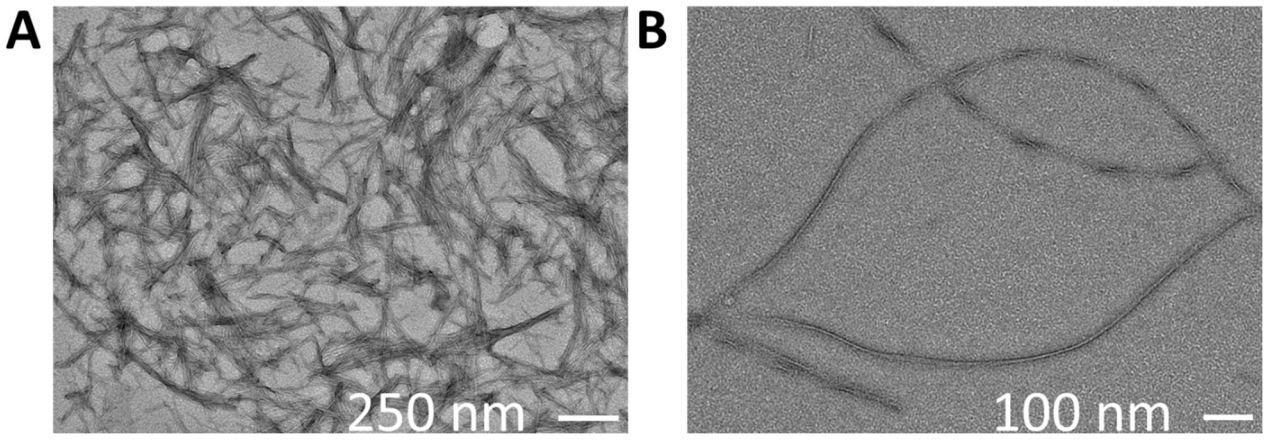

Figure 15. Representative TEM images of KFE9 assembled in 10mM pH4.0 acetate at 3mg/mL under ambient conditions for 1 week (A) and after annealing (B)), samples are stained with 1% UA. Short bundles of thin filaments formed into ill-defined aggregates and clumps in the unannealed sample. Thin, twisted filaments were observed in the annealed sample.

KFE9 assembled for 6 weeks showed two distinct populations of supramolecular structures: thin twisted fibrils and larger straight filaments that appear to have a cylindrical morphology despite the lack of a clearly visible lumen. Twisted filaments bear structural similarities to the observed twisted fibrils of Amyloid β peptide (Aβ) amyloid fibrils assembled in vitro[19]. The straight filaments have a mean width of 24 nm with a high standard deviation of 3 nm indicating that there is a significant degree of fluctuation in diameter between filaments.

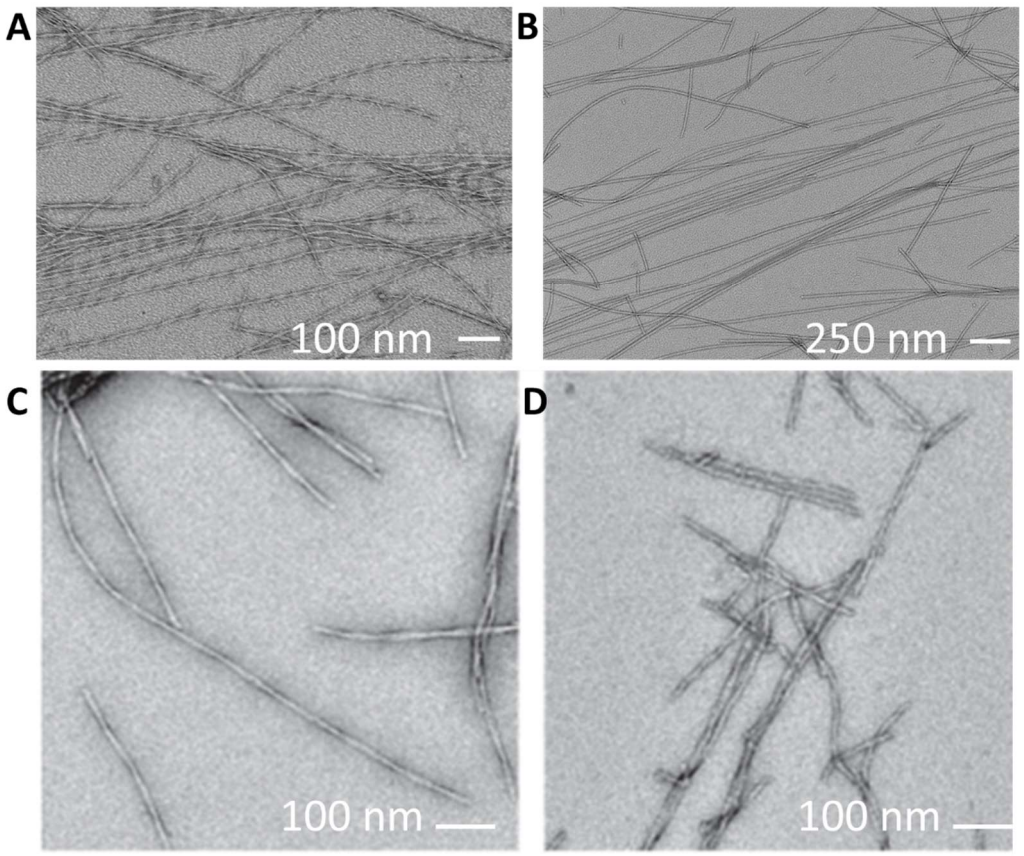

Figure 16. Representative TEM images of KFE9 allowed to assemble for 6 weeks in pH4 acetate at room temperature and stained with 1% PTA. Two distinct morphologies emerged: thin twisted filaments (A) resembling twisted amyloid fibrils observed in the morphologies of Aβ amyloid fibrils assembled in vitro (C) as opposed to Aβ amyloid fibrils purified ex vivo (D), and large, straight filaments (B) bearing cylindrical character but lacking well-defined lumens. Images of Aβ-fibrils are adapted from data published by Kollmer *et al*[19].

Samples assembled in higher pH buffers were also examined by TEM to investigate trends in the supramolecular morphology of each peptide with increasing pH. Samples were transferred onto copper grids 3 hours after assembly for analysis. Overall, TEM data

corroborated trends observed by CD for RFE8 and KFE7. RFE8 assembled into helical ribbons and tubes in pH5.0 and pH6.0 buffers and showed little to no assembly at pH7.0 and weak indications of helical ribbons at pH8.0. KFE7 formed assemblies in all buffers, with short, brittle filaments and sheets forming in every buffer condition. Supramolecular structures formed by KFE7 showed a tendency to stick to each other.

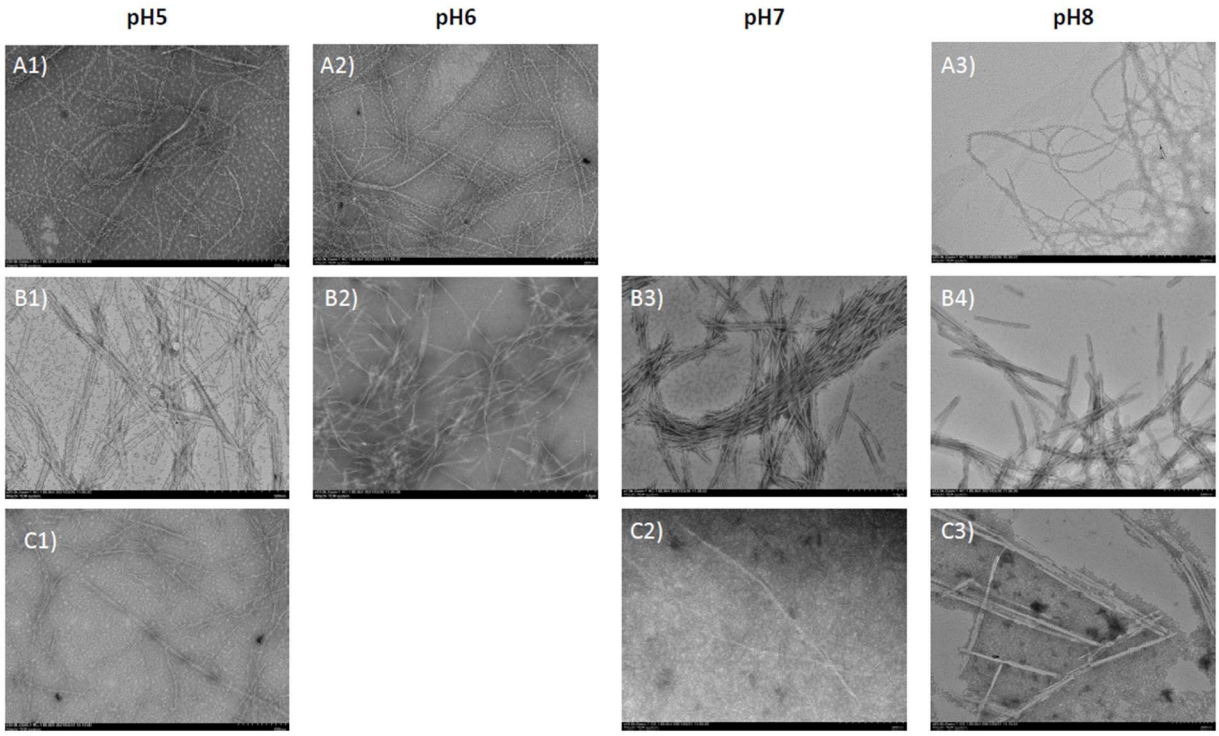

Figure 17. Representative TEM images for samples of RFE8 (A1-3), KFE7 (B1-4), and KFE9 (C1-3) assembled at 3mg/mL in buffers titrated to pH5.0, pH6.0, pH7.0, and pH8.0. Samples were incubated at room temperature for 3 hours before staining by 1% PTA and imaging. Blank squares indicate that no visible structures were visualized by TEM.

Examination of KFE9 by TEM revealed formation of thin filaments and twisted fibrils in pH5.0 acetate, but very little supramolecular assembly was observed in other buffers. Although

TEM data was initially inconclusive, high pH assemblies of KFE9 were noticeably more viscous compared to RFE8 and KFE7 after several weeks of assembly. Additionally, because KFE9 assembled in pH4.0 acetate had initially showed little to no assembly on TEM after 1 week of incubation, but had developed distinct supramolecular architectures after 6 weeks, higher pH assemblies of KFE9 were reimaged after 8 weeks of incubation to ascertain if supramolecular structures had developed. Although assemblies in pH5.0 and pH6.0 buffer continued to display an absence of supramolecular structure, large bundles of thin filaments were observed throughout samples of KFE9 assembled at pH7.0 and pH8.0.

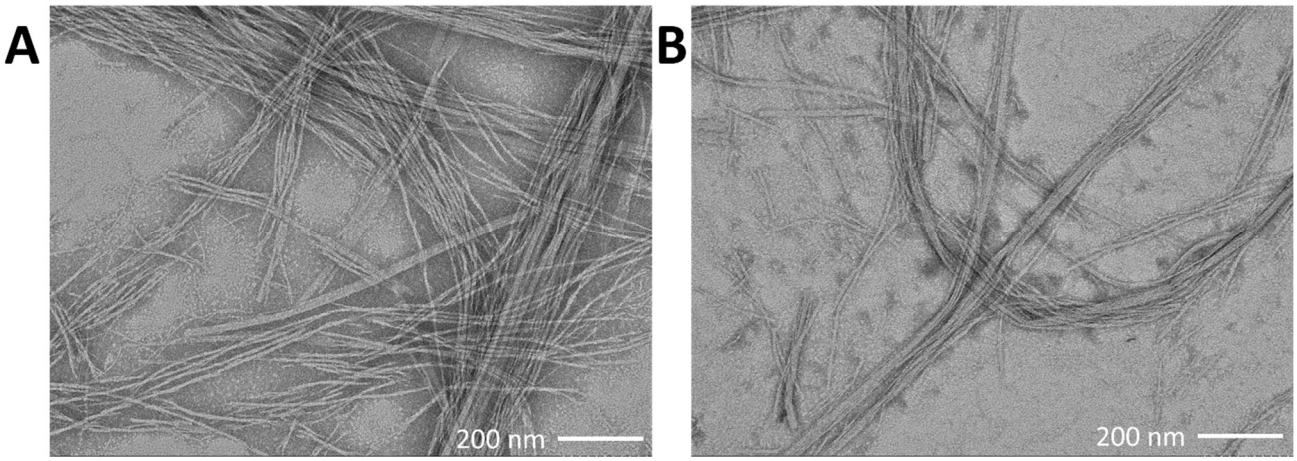

Figure 18. Representative TEM images of KFE9 assembled at room temperature for 8 weeks in pH7.0 MOPS (A) and pH8.0 TAPS (B) stained with 1% PTA. Large bundles of filaments of varying length and width were dispersed throughout the samples.

Conclusion:

The vast collection of morphologies that have emerged from small mutations in the sequence of the simple octapeptide KFE8 truly illuminates the chaotic nature of protein and peptide folding. It is known that β-sheet forming peptides can display a wide range of polymorphisms by virtue of the many orientations that parallel and antiparallel β-sheets can adopt[7]. The Conticello lab has previously identified that even small changes to the assembly environment of KFE8 can lead to heterogenous mixtures of novel supramolecular structures[12]. This work continues in that vein to show that even well-understood assembly paradigms for the formation of β-sheets through polar sequence patterning and alternating hydrophobic and hydrophilic peptide sequences are not predominant enough to control or even predict the architecture of higher order assemblies. The three peptides studied in this project displayed a wide range of physiochemical properties including: sensitivity to pH, rate of assembly, ability to induce viscosity, and the number and variety of supramolecular morphologies that could be observed across a broad range of assembly conditions.

Of these three analogues of KFE8, only RFE8 was able to replicate the self-assembly behavior of its parent sequence. Although RFE8 readily formed helical ribbons and tubes of slightly wider diameter than KFE8 when left to assemble in ambient conditions, the mixture of structures failed to converge into a single prevailing morphology even after multiple weeks of incubation. Although ribbons were absent in the annealed samples of RFE8, the presence of wider sheet-like filaments were observed in tandem with nanotube. RFE8 was shown to be sensitive to environments with pH higher than 6, after which assembly of secondary and higher structure is severely abrogated.

KFE7 displayed rapid and consistent self-assembly at a secondary structural level across the gamut of pH levels measured but was slow to assemble into higher order structures. Virtually no assembly occurred within a week of assembly in pH4 acetate even after annealing, although large filaments of variable width were eventually observed after 6 weeks of ambient incubation. Short filaments with a tendency to aggregate and collect were observed forming at all pH levels, and the measured ellipticity of secondary structural characteristics was highest in samples assembled with pH8 buffer. Whereas RFE8 assembly was discouraged with increasing pH, KFE7 was either insensitive to or even preferred higher pH environments for self-assembly.

KFE9 was also significantly slower at forming higher order structures than RFE8, but nucleation of bundled filaments was observed after 1 week of assembly in pH4 acetate and twisted fibrils morphologies did appear when KFE9 was annealed. After 6 weeks of incubation at room temperature, two distinct morphologies emerged including twisted fibrils that resembled in vitro assembled Aβ amyloid fibrils, the primary component of plaque buildup in the brains of patients with Alzheimer's Disease[19]. Larger rod-like filaments were also observed, but without further structural analysis their exact characteristics are impossible to determine. KFE9 displayed extremely limited assembly in pH5.0 and pH6.0 buffers and was slow to assemble at pH7.0 and pH8.0. However, KFE9 notably induced significant viscosity in higher pH buffers, and large networks of bundled fibers were observed forming after several weeks in pH7 and pH8 buffer.

This study proves that increasing the hydrophilic character of KFE8 via truncation of hydrophobic residues or insertion of hydrophilic residues severely alters the self-assembly behavior of resulting amphiphilic peptides. Increasing hydrophilicity of KFE8 via mutation from lysine to arginine does not abolish self-assembly of helical ribbons and nanotubes, but the morphology of resulting structures is still distinct from KFE8. Although KFE7 and KFE9 do

exhibit self-assembly, the assemblies are of entirely disparate morphologies. Although each of the peptides studied during this project exhibited high β-sheet content, which corroborates the contribution of polar sequence patterning and alternating polar and nonpolar residues towards self-assembly behavior, the hierarchical progression of assembly past the secondary level of structural organization introduces too many uncontrollable variables for accurate prediction of supramolecular morphology from sequence. The paradigms identified in KFE8 that direct supramolecular assembly are limited in scope, and higher order structural organization is not resilient to even single residue insertions or deletions. Sequence to structure control of β-sheet assemblies remains a challenge in the field of biomaterial science, and it has become increasingly evident that even the simplest folding archetypes govern an extremely narrow range application.

Materials and Methods:

All chemical reagents were purchased from Fisher Scientific, Inc. (Pittsburgh, PA), Anaspec, Inc (Fremont, CA) or Sigma-Aldrich Chemical Co. (St. Louis, MO) unless otherwise specified and used without further purification.

Peptide Synthesis and Assembly: RFE8 (Ac-FRFEFRFE-NH_2), KFE7 (Ac-KFEFKFE-NH_2), and KFE9 (Ac-KFEFQFKFE-NH_2) peptides were obtained from GenScript USA Inc (Piscataway, NJ) as the N-acetyl, C-amide derivative at >95% purity by analytical HPLC. Stock solutions of the KFE8 peptide were prepared by solubilizing purified, lyophilized peptide powder in sodium acetate buffer (10 mM, pH 4.0) and (10 mM, pH 5.0), 2-ethanesulfonic acid (MES) buffer (10mM, pH 6.0), 3-morpholinopropane-1-sulfonic acid (MOPS) buffer (10mM, pH 7.0) and tris(hydroxymethyl)methylamino]propanesulfonic acid (TAPS) buffer (10mM, pH 8.0) in a ratio of 3mg of powder per 3mL of buffer after which solutions were vortexed (5-10 minutes) to

ensure solubilization. The solutions were allowed to either incubate at ambient temperature or were subjected to the following annealing protocol in a thermal cycler: (1) rapid heating to 90 deg. C for 30 min and (2) cooling to 25 deg. C at a rate of 0.2 deg. C/min.

Circular Dichroism Spectropolarimetry: CD measurements were taken on a Jasco J-1500 CD Spectropolarimeter using a 0.20 mm quartz cuvette (Hellma USA Inc, Plainveiw, NY). Signals were measured three times consecutively, averaged, and corrected with a blank spectrum of the corresponding buffer. Spectra were taken with a scan rate of 100nm/min from 190-260nm with a bandwidth of 2nm and data pitch of 0.2nm.

Negative Stain and TEM analysis: TEM grids were prepared with assembled samples of peptide at 3mg/mL concentration. 4μL of each sample were deposited onto 200-mesh carbon-coated copper grid (Electron Microscopy Services, Hatfield, PA) and allowed to incubate for 90 seconds. Excess liquid was wicked away and 4μL of 1% Uranyl Acetate solution or 1% Phosphotungstic acid was deposited onto the grid surface and incubated for 90 seconds. Remaining moisture was wicked away, and electron micrograph images were collected on a Hitachi HT-7700 transmission electron microscope. The microscope is equipped with a tungsten filament, an AMT CCD camera, and operates at an accelerating voltage of 80kV.

References:

1. Bowerman, C.J., and Nilsson, B.L. (2012). Review self-assembly of amphipathic b-sheet peptides: insights and applications. Pept. Sci. 98, 169–184.
2. Pauling, L.; Corey, R. B. Proc Natl Acad Sci USA 1953, 39, 253–256.
3. Hwang W. Marini D.M. Zhang S. et al. Supramolecular structure of helical ribbons self-assembled from a β-sheet peptide. J. Chem. Phys. 2003; 118: 389-397 https://doi.org/10.1063/1.1524618
4. Marini, D. M.; Hwang, W.; Lauffenburger, D. A.; Zhang, S.; Kamm, R. D. Left-Handed Helical Ribbon Intermediates in The Self Assembly of A β-Sheet Peptide Nano Letters 2002, 2, 4, 295–299 Publication Date: February 21, 2002, https://doi.org/10.1021/nl015697g
5. Michael R. Caplan, Elissa M. Schwartzfarb, Shuguang Zhang, Roger D. Kamm, Douglas A. Lauffenburger, Control of self-assembling oligopeptide matrix formation through systematic variation of amino acid sequence, Biomaterials, Volume 23, Issue 1, 2002, Pages 219-227, ISSN 0142-9612, https://doi.org/10.1016/S0142-9612(01)00099-0.
6. Nelson, R., Sawaya, M. R., Balbirnie, M., Madsen, A. Ø., Riekel, C., Grothe, R., & Eisenberg, D. (2005). Structure of the cross-beta spine of amyloid-like fibrils. Nature, 435(7043), 773–778. https://doi.org/10.1038/nature03680
7. Eisenberg DS, Sawaya MR. Structural Studies of Amyloid Proteins at the Molecular Level. Annu Rev Biochem. 2017 Jun 20; 86:69-95. doi: 10.1146/annurev-biochem-061516-045104. Epub 2017 Jan 3. PMID: 28125289.

8. Morris K, Serpell L. From natural to designer self-assembling biopolymers, the structural characterisation of fibrous proteins & peptides using fibre diffraction. Chem Soc Rev. 2010 Sep;39(9):3445-53. doi: 10.1039/b919453n. Epub 2010 Jul 29. PMID: 20668734.
9. Micsonai A, Bulyáki É, Kardos J. BeStSel: From Secondary Structure Analysis to Protein Fold Prediction by Circular Dichroism Spectroscopy. Methods in Molecular Biology (Clifton, N.J.). 2021; 2199:175-189. DOI: 10.1007/978-1-0716-0892-0_11. PMID: 33125651.
10. Tycko R. Solid-state NMR studies of amyloid fibril structure. Annu Rev Phys Chem. 2011; 62:279-99. doi: 10.1146/annurev-physchem-032210-103539. PMID: 21219138; PMCID: PMC3191906.
11. Kovacs JM, Mant CT, Hodges RS. Determination of intrinsic hydrophilicity/hydrophobicity of amino acid side chains in peptides in the absence of nearest-neighbor or conformational effects. Biopolymers. 2006;84(3):283-97. doi: 10.1002/bip.20417. PMID: 16315143; PMCID: PMC2744689.
12. Fengbin Wang, Ordy Gnewou, Shengyuan Wang, Tomasz Osinski, Xiaobing Zuo, Edward H. Egelman, Vincent P. Conticello, Deterministic chaos in the self-assembly of β sheet nanotubes from an amphipathic oligopeptide, Matter, Volume 4, Issue 10, 2021, pages 3217-3231, ISSN 2590-2385, https://doi.org/10.1016/j.matt.2021.06.037.
13. Cryo-EM of Helical Polymers, Fengbin Wang, Ordy Gnewou, Armin Solemanifar, Vincent P. Conticello, and Edward H. Egelman, Chemical Reviews Article ASAP DOI: 10.1021/acs.chemrev.1c00753
14. A. Aggeli, I.A. Nyrkova, M. Bell, R. Harding, L. Carrick, T.C.B. McLeish, A.N. Semenov, N. Boden, Hierarchical self-assembly of chiral rod-like molecules as a model

for peptide b-sheet tapes, ribbons, fibrils, and fibers, Proc. Natl. Acad. Sci. U. S. A. 98 (2001) 11857e11862.

15. Tuning β-Sheet Peptide Self-Assembly and Hydrogelation Behavior by Modification of Sequence Hydrophobicity and Aromaticity, Charles J. Bowerman, Wathsala Liyanage, Alexander J. Federation, and Bradley L. Nilsson Biomacromolecules 2011 12 (7), 2735-2745 DOI: 10.1021/bm200510k
16. Caplan MR, Moore PN, Zhang S, Kamm RD, Lauffenburger DA. Self-assembly of a beta-sheet protein governed by relief of electrostatic repulsion relative to van der Waals attraction. Biomacromolecules. 2000 Winter;1(4):627-31. doi: 10.1021/bm005586w. PMID: 11710192.
17. Lim, Y.-b.; Lee, E.; Lee, M. Cell-Penetrating-Peptide-Coated Nanoribbons for Intracellular Nanocarriers. Angew. Chem., Int. Ed. 2007, 46, 3475– 3478, DOI: 10.1002/anie.200604576
18. Tuning the Self-Assembly of Short Peptides via Sequence Variations, Yurong Zhao, Jiqian Wang, Li Deng, Peng Zhou, Shengjie Wang, Yanting Wang, Hai Xu, and Jian R. Lu Langmuir 2013 29 (44), 13457-13464 DOI: 10.1021/la402441w
19. Kollmer, M., Close, W., Funk, L. et al. Cryo-EM structure and polymorphism of Aβ amyloid fibrils purified from Alzheimer's brain tissue. Nat Commun 10, 4760 (2019). https://doi.org/10.1038/s41467-019-12683-8

Chapter 3: Development of Novel Self-Assembling β-Peptide Foldamer Oligopeptides

Introduction and Design:

The term "Foldamer" is used broadly in protein science to describe any class of polymer with the tendency to fold into specific, compact configurations in solution[1-3]. Unfortunately, native peptides are notoriously bad at assembling compactly, and although the intricate cooperative folding of large globular proteins is a testament to the natural artistry of living systems, brevity is the soul of wit, and none are wittier than biophysical chemists [citation needed]. As such, foldamer research is focused on producing synthetic biomimetic building blocks inspired by natural molecular scaffolds which can fold neatly, succinctly, and predictably into useful secondary structures that are otherwise inaccessible to natural biomolecules[1-3].

Among the many classes of foldamers, derivatives of amino acids containing a homologated backbone, β-peptides, have emerged at the forefront of foldamer research due to their propensity to organize into unique classes of secondary structures. These structures include multiple forms of helices, sheets, and turns[4], while retaining the biochemical flexibility of the side-chain alphabet. Classical β-peptides can be separated into two categories: β^3-peptides possess side chains placed nearest to the amine whereas β^2-peptides have side chains located nearest to the carbonyl of the extended 3-carbon backbone. Further development of β-peptide archetypes has also yielded classes of disubstituted peptides with two organic appendages and cyclic homologated peptides with more constrained angular geometries (Figure 19.).

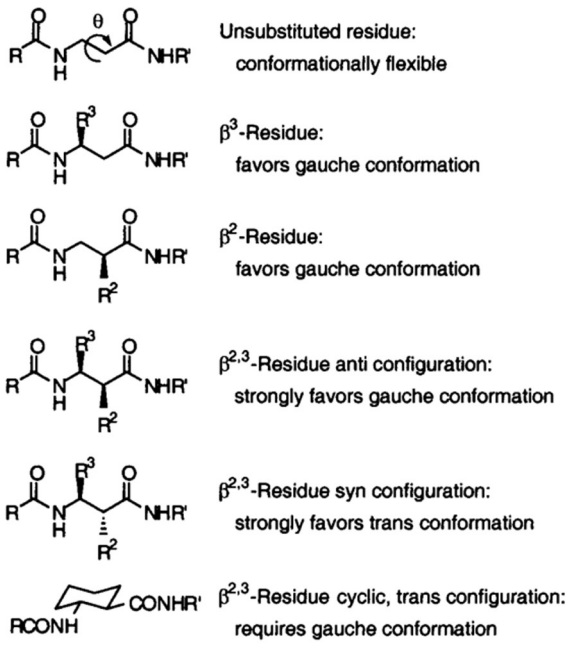

Figure 19. Categories of β-peptides based on their substituents, adapted from work by Cheng, *et al.*[3]

Oligomers composed entirely of β^3-$_L$-peptides can adopt several unique helical architectures which offer diverse functionalities that α-helices cannot. The nomenclature for β-peptide helices is derived from the number of atoms in the stabilizing hydrogen bonded rings associated with each helical form (Figure 20.). Chief amongst the β-peptide helices is the 14-helix, which adopts a stunningly simple conformation with 3 residues per turn stabilized by hydrogen bonding between backbone carbonyl oxygens and amide hydrogens at the *i -2* position[3]. The result is a left-handed (for β^3-$_L$-peptides) helix with residues arranged in 120° intervals producing a helix with 3 distinct faces. Early work in the foldamer space sought to encourage the formation of 14-helical character in aqueous buffers via intramolecular salt bridges[5,6] and inclusion of cyclic (β^2- β^3) amino acids[7,8].

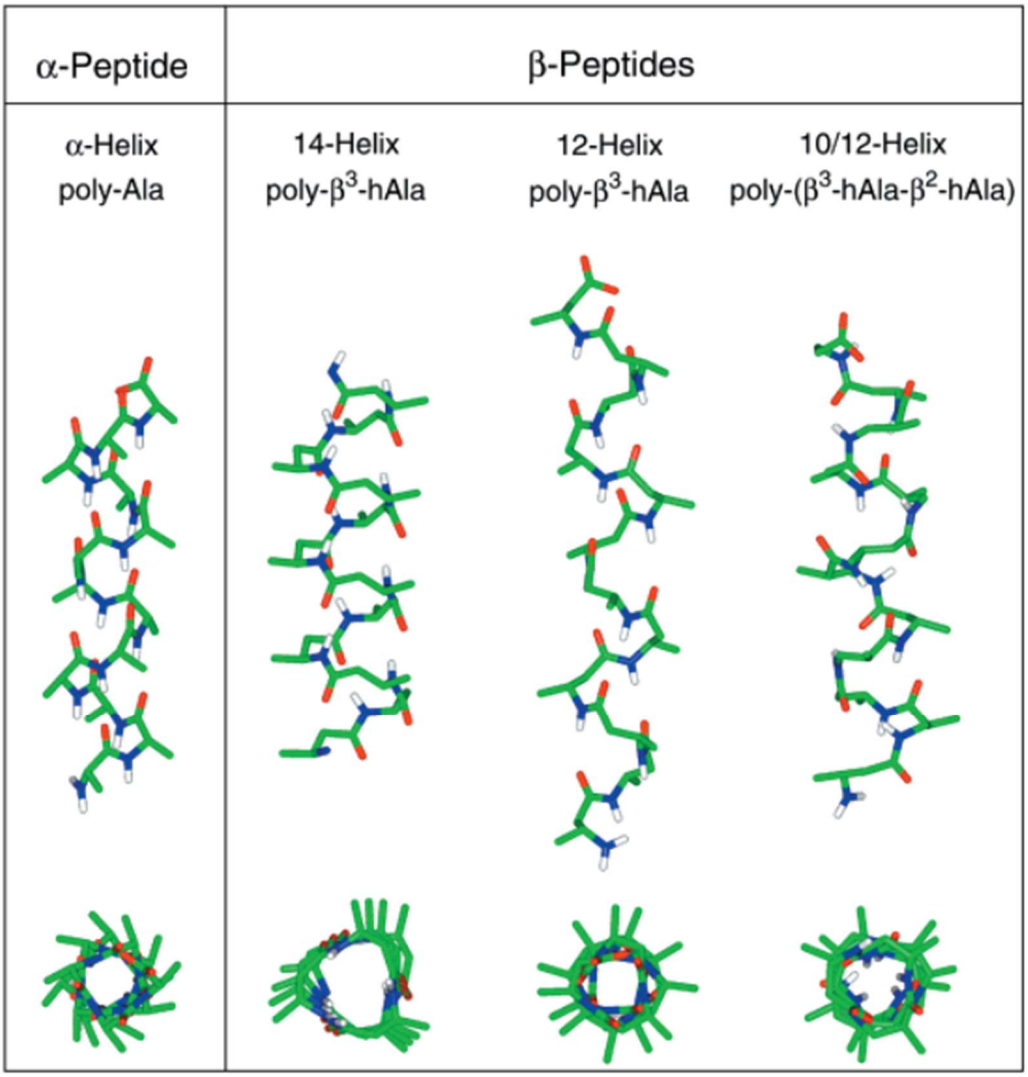

Figure 20. Structures of the 14-helix, 12-helix, and 10/12 helix compared to a traditional α-helix, adapted from Cheng *et al.*[3]

Regarding the design of soluble 14-helical β^3-$_L$-peptides, additional consideration must be made regarding the macrodipole of the helix. In α-helical designed sequences, it is understood that a macrodipole is formed by the directed orientation of hydrogen bonds along the length of the helix with a partial positive charge near the N-terminus and a partial negative charge forming

near the C-terminus. A stabilizing effect is thereby achieved from placing negatively charged residues near the N-terminus and positively charged residues near the C-terminus to neutralize accumulation of partial charge[9]. In the 14-helix, the orientation and direction of hydrogen bonding along the helix is reversed and thus a reverse macrodipole forms with partial negative character near the N-terminus and partial positive charge building at the C-terminus. Neutralization of the 14-helix macrodipole through strategic placement of positively charged residues near the N-terminus and negatively charged residues near the C-terminus thereby improves helical stability in aqueous conditions.[5]

Although numerous examples of 14-helical β-peptides have been designed, we were intrigued by a particularly interesting set of self-assembling helical β-peptides driven primarily by (S,S)-trans-2-aminocyclohexanecarboxylic acid (S,S-ACHC) which self-assemble into nanotubes as described by the Gellman group[7,8] (Figure 21.). Structural analysis of the resulting supramolecular assemblies has exciting implications for rationalizing the hierarchical assembly of non-native oligopeptides for use in *de novo* peptide design. If compact folding of β-peptide foldamers into secondary structures helps to reduce the number of polymorphism inducing events, perhaps more accurate sequence to structure correlation can be achieved outside the realm of natural amino acids. High resolution cryo-EM structural analysis has not yet been employed for the study of β-peptide derived supramolecular sequences, making this project the first of its kind.

The peptides characterized by the Gellman group are amphipathic decapeptide sequence isomers designed according to a 14-helical principle with different arrangements of hydrophobic and hydrophilic residues. Iso-A (H_2N-(β^3K-β^3F-ACHC)$_3$-β^3Y-NH_3^+) has a repeating triad in phase with the helical register of the 14-helix and was predicted to produces a globally

amphiphilic helix with segregation of hydrophilic groups onto a single face of the resulting trilateral nanostructure. Peptide A (H_2N-β^3K-β^3F-ACHC-ACHC-β^3K-β^3F-ACHC-β^3F-β^3K-β^3Y-NH_3^+), which we refer to as Gellman A, is designed to distribute the charged β^3K residue onto all three faces of the 14-helix, making it non-globally amphiphilic. Surprisingly, Gellman A readily self assembles into nanotubes and forms a lyotropic liquid crystal in water whereas iso-A fails to do either.

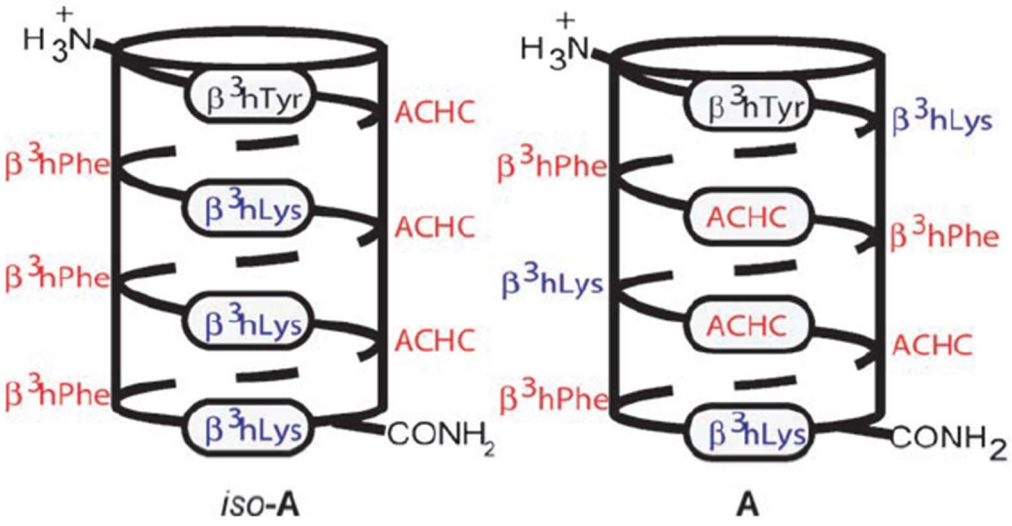

Figure 21. Cylindrical representation of the predicted 14-helix architecture of iso-A and A adapted from Pomerantz *et al.*[8]

Further iterations of Gellman A intended to probe the importance of specific residues revealed that knockout of aromaticity completely annuls observed liquid crystallinity of the peptide, whereas substitution of β^3K with hydrophilic groups of negative or neutral charge decreased the minimum concentration required for formation of the liquid crystal phase. Both iso-A and A presented strong 14-helical CD spectra, refuting the possibility of an alternative

secondary structural basis for self-assembly. These bizarre observations are difficult to explain by classical understandings of hierarchical assembly in natural polypeptides.

Herein we proposed two analogues of the Gellman A and iso-A peptides that employ polar sequence patterning to establish salt-bridges at the charged interface of iso-A and replace ACHC residues, which bias the formation of 14-helical structures by their constrained conformations, with β^3-Phe (Table 3.). β-lys maintains the use of β^3-Lys, and introduces β^3-Glu residues. Cheng and DeGrado identified instances where salt bridge interactions between β^3-Lys/β^3-Glu can improve secondary structure formation of β-peptides in water[10]. β-arg mutates the β^3-Lys residues to β^3-Arg to verify that the effect of positively charged sidechains is generalizable and not residue specific. With the introduction of negatively charged residues, we carefully placed them closer to the C-terminus in order to appropriately neutralize the 14-helix macrodipole. Literature suggests that capping of the N-terminus via acetylation inhibits 14-helix formation by occluding the positively charged terminal amine from further neutralizing the 14-helix macrodipole[5], so we also synthesized analogues of β-lys and β-arg without n-terminal acetylation.

Peptide	Sequence and helical register 1231231231
Iso-A	H2N - KFXKFXKFXY - NH3+
A	H2N - KFXXKFXFKY - NH3+
β-lys	H2N - EFFKFFEFFK - Ac
β-arg	H2N - EFFRFFEFFR - Ac
β-lys (uc)	H2N - EFFKFFEFFK - NH3+
β-arg (uc)	H2N - EFFRFFEFFR - NH3+

Table 3. List of relevant sequences aligned according to the register of the 14 helix. X represents S,S ACHC residues. Iso-A and A are derived from work by Pomerantz *et al.*[7,8] β-lys and β-arg

and the uncapped versions are listed in comparison. Positively charged polar residues are highlighted in red, negatively charged polar residues are highlighted in blue.

At this point it is important to take a step backwards to admire the amount of care and thought that was put into the highly specific sequence order and selection of residues that were incorporated after piecing together the many fragments of emerging data surrounding β-peptide design. Throughout this work, it is perhaps understated that the calculated design of each individual peptide has been the result of meticulous deliberation and analysis. The Conticello lab takes pride in precisely identifying key experimental gaps in the vast landscape of peptide science and answering them with rigor and delicacy. In the emerging field of β-peptide foldamer assembly, we must be cautious not to overlook any small details that could prove to be critical in building a stable set of foundational principles regarding β-peptide behavior and design. The designs that Dr. Conticello have elaborated are highly intentional and deserving of respect.

It is also important that we detail a few specific moments of chemistry history that I have selected to illustrate a forthcoming idea. In 1928, Alexander Fleming returned to his laboratory after a vacation to discover a rare species of mold that that contaminated a petri dish. This mold, a strain of Penicillium notatum, appeared to secrete a substance into the surrounding dish which inhibited the growth of bacteria. This was the discovery of penicillin, the world's first antibiotic.[11] In 1903 Edward Benedictus knocked a glass flask onto the floor of his laboratory. Instead of shattering into a potential safety hazard, Benedictus noticed that despite being cracked and broken, the glass had retained its shape and refrained from causing a mess. This glassware had not been properly cleaned by his lab assistant, and the inside had been coated with a solution of cellulose nitrate. This series of accidents led to the discovery of safety glass.[12,13] These

moments of chemical history highlight that important discoveries can emerge as a result of accidental and frivolous conduct in a laboratory setting.

During the initial synthesis of β-lys via microwave assisted solid-phase peptide synthesis, an erroneous peptide sequence, hereafter named β-Happy Accident (β-HA), was mistakenly prepared and submitted for synthesis. It may be recalled that the order of the peptide sequence for β-lys and β-arg was intentional and important for stabilization of the 14-helix. β-HA was the result of entering the sequence for β-lys backwards, followed immediately by an unforced malfunction of the peptide synthesizer which prevented the ligation and coupling of the last glutamate residue of the reversed β-lys sequence and left the N-terminus uncapped. The sequence of β-HA is thus (H_2N-β^3K-β^3F- β^3F-β^3E-β^3F-β^3F- β^3K-β^3F- β^3F-NH_3^+). Purification and assembly of β-HA proceeded until mass spectrometry revealed the erroneous mass.

Coincidentally, although the correct sequences of β-lys, β-lys (uc), β-arg and β-arg (uc) were later synthesized without error, purification of the crude peptide product failed because all of the β-peptides were virtually insoluble in water with 0.1% TFA, HPLC water, acetonitrile with 0.1% TFA, acetonitrile, methanol, ethanol, isopropanol, acetone, DMSO, DMF, and TFE even after sonication and heating (Figure 22.). Crude mass spectrometry confirmed the presence of the desired product (Figure 23.), but without the ability to solubilize the products or purify them, the sequences were abandoned, and further characterization of β-HA, which was soluble in aqueous buffer, proceeded.

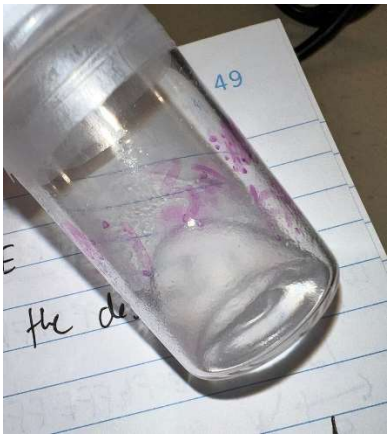

Figure 22. Representative image of β-lys suspended in HPLC water with .1% TFA. Attempts to solubilize β-lys, and β-arg were futile across a screen of solvents. Even after serial dilution the solution remained turbid, and significant quantities of debris precipitated out.

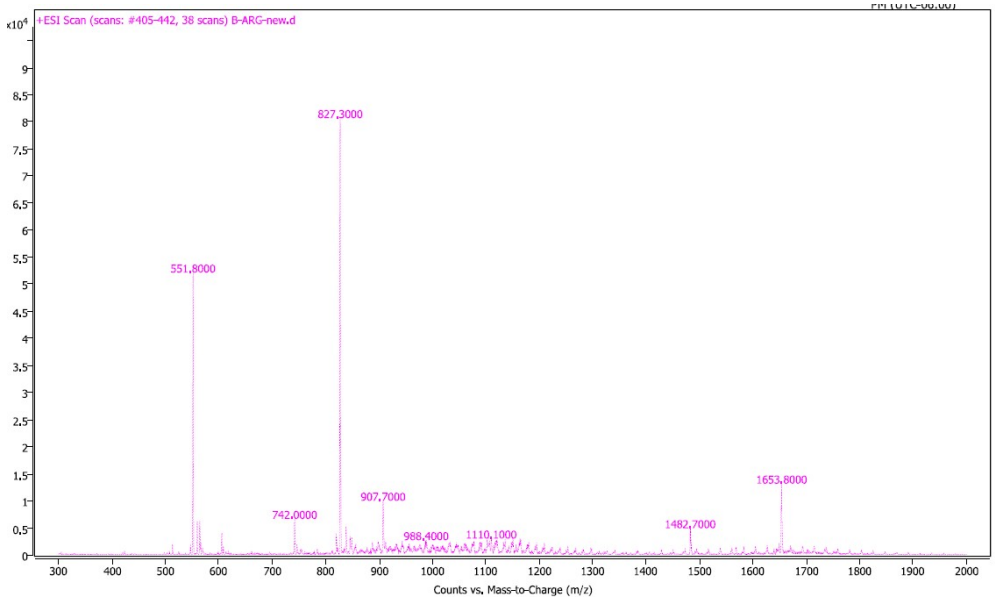

Figure 22. Representative ESI mass spectroscopy reading of crude β-Arg (MW: 1653).

Results and Discussion:

Peptide Synthesis and Assembly: β-HA was synthesized using microwave assisted solid-phase peptide synthesis. β-HA was purified using reversed-phase HPLC on a C-18 column followed by lyophilization to yield a white powder. The identity of β-HA was confirmed using ESI mass spectrometry. Conditions for assembly were screened across multiple buffers to identify the optimal pH for self-assembly. Peptides were dissolved at 3mg/mL of aqueous buffer (10mM TFA pH 2.0, 10mM acetate pH 4.0, 10mM MOPS pH 7.0, 10mM CAPS pH 10.0) and allowed to assemble in ambient conditions at room temperature. Aliquots of pH 2.0 TFA and pH 4.0 acetate buffers were also taken and annealed both directly after assembly and after 1 week of assembly at room temperature by rapidly heating in a thermocycler to 90°C for 30 minutes and cooling to 25°C at a rate of 0.2°C/minute.

Circular Dichroism: CD spectra of β-HA assembled in ambient conditions for 12 weeks were analyzed to verify 14-helix content (Figure 24.) Strength of 14-helical character is estimated from CD spectra based on the strength of minima at 215 nm[3].

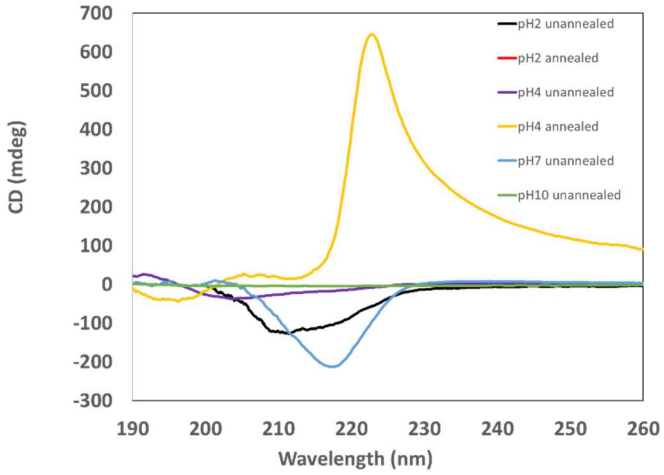

Figure 24. Overlaid CD spectra of β-HA assembled at 3mg/mL at room temperature for 12 weeks in 10mM TFA pH 2.0 (black), 10mM acetate pH 4.0 (purple), 10mM MOPS pH 7.0 (blue), 10mM CAPS pH 10.0 (green), and annealed in 10mM TFA pH 2.0 (red) and 10mM acetate pH 4.0 (yellow)

β-HA assembled in pH2 buffer under ambient conditions displays a single minimum at 211nm, which is slightly blue shifted relative to the position of a traditional 14 helix. Ambient assemblies in pH4 buffer were even more significantly blue shifted, with a maximum at 192 nm and a minimum at 203 nm that refutes the likelihood of 14 helix formation. Ambient pH7 assemblies displayed the characteristic minima at 217nm that is strongly indicative of pure 14 helical content. The CD spectra of β-HA assembled in ambient pH10 buffer showed virtually no secondary structural content.

β-HA annealed in pH2 buffer showed no indication of secondary structure formation. However, the CD spectra of annealed β-HA in pH4 acetate deviates prominently from the rest of the samples, with an extremely pronounced peak at 223nm that suggests an inversion towards a right-handed secondary morphology.

Transmission Electron Microscopy: Unannealed β-HA was first examined by TEM after three days of assembly at room temperature in 10mM pH2, pH4, pH7, and pH10 buffer. Samples were stained with 1% UA. (Figure 25.). The immediate obvious presence of massive helical ribbons was shockingly clear in pH2 and pH4 buffer conditions. Ribbons were less defined and less helical in pH7 and pH10 buffers, still easily identifiable and clearly present. Smaller, thinner filaments were also dispersed throughout all of the samples. The dimensions of individual ribbons were highly varied, and in some cases the widths of ribbons appeared to taper off and disappear.

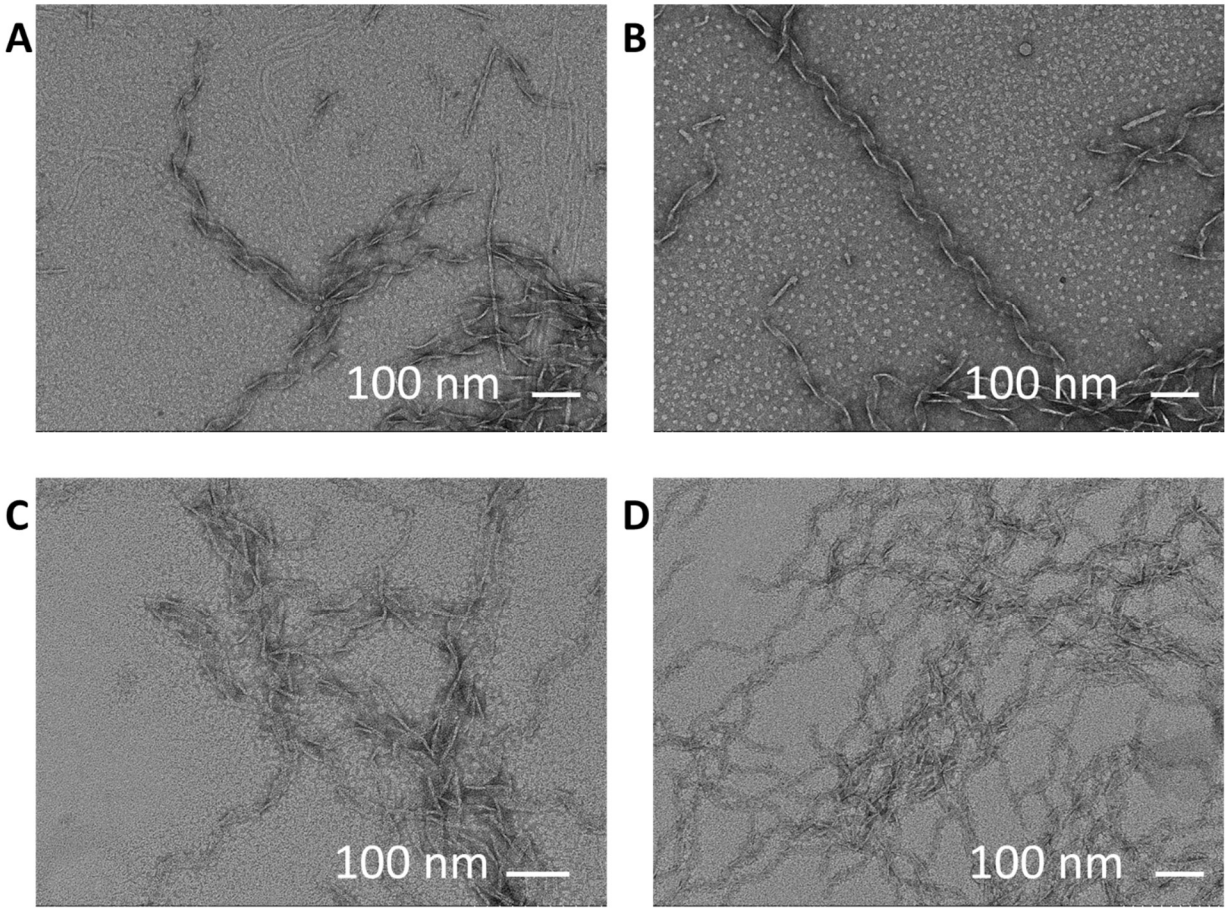

Figure 25. TEM micrographs of Unannealed β-HA assembled in pH2 (A), pH4 (B), pH7 (C), and pH10 (D) buffers in ambient conditions for 3 days. Samples were negatively stained with 1% UA.

Aliquots of the pH2 samples that had already incubated in ambient conditions were annealed and imaged under TEM (Figure 26.). The previously observed filaments and ribbons persisted, but ribbons were observed tightening to form straight tapes. It was abundantly clear that the prevailing morphology was the thin filaments that formed dense meshes surrounding the tubes and ribbons.

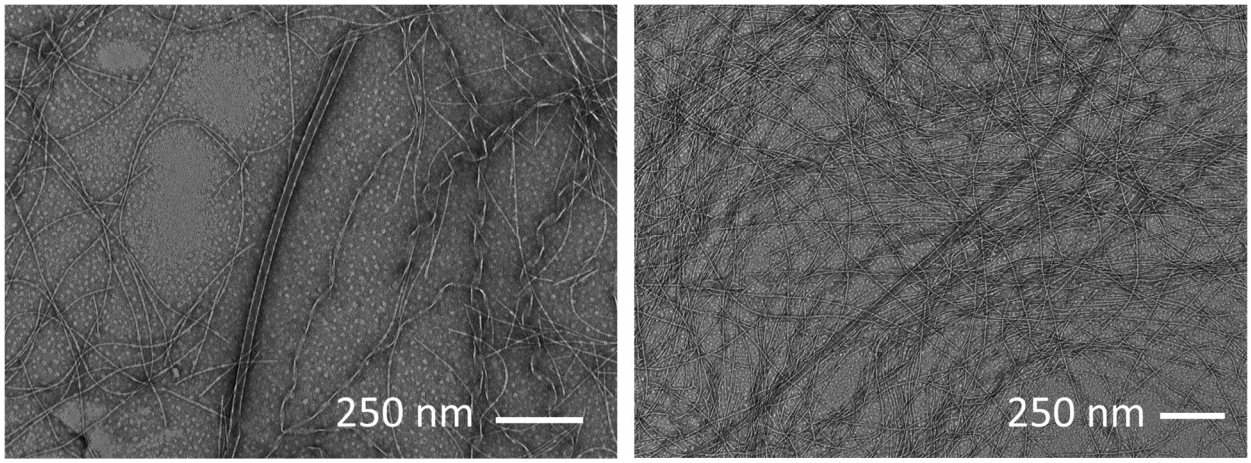

Figure 26. Representative TEM images of β-HA assembled at room temperature in 10mM pH 2.0 buffer for a week and then annealed. A heterogenous mixture of supramolecular morphologies can be seen overlaid with each other.

Concerns regarding the efficacy of the annealing process after allowing β-HA to assemble and nucleate into ordered structures at room temperature were raised, so fresh assembly of β-HA was conducted in pH2 and pH4 buffer followed immediately by annealing (Figure 27.). The resulting peptides were of a drastically different morphology than the unannealed peptide, with dense aggregates of short filaments and longer twisted fibrils being the primary supramolecular structures observed. The shift in morphologies corroborates the massive difference in CD spectra between the freshly annealed and unannealed samples at pH4. The fact that the helical ribbons did not denature after annealing suggests that they are tolerant to high temperature conditions, even if annealing immediately after assembly prevents their formation.

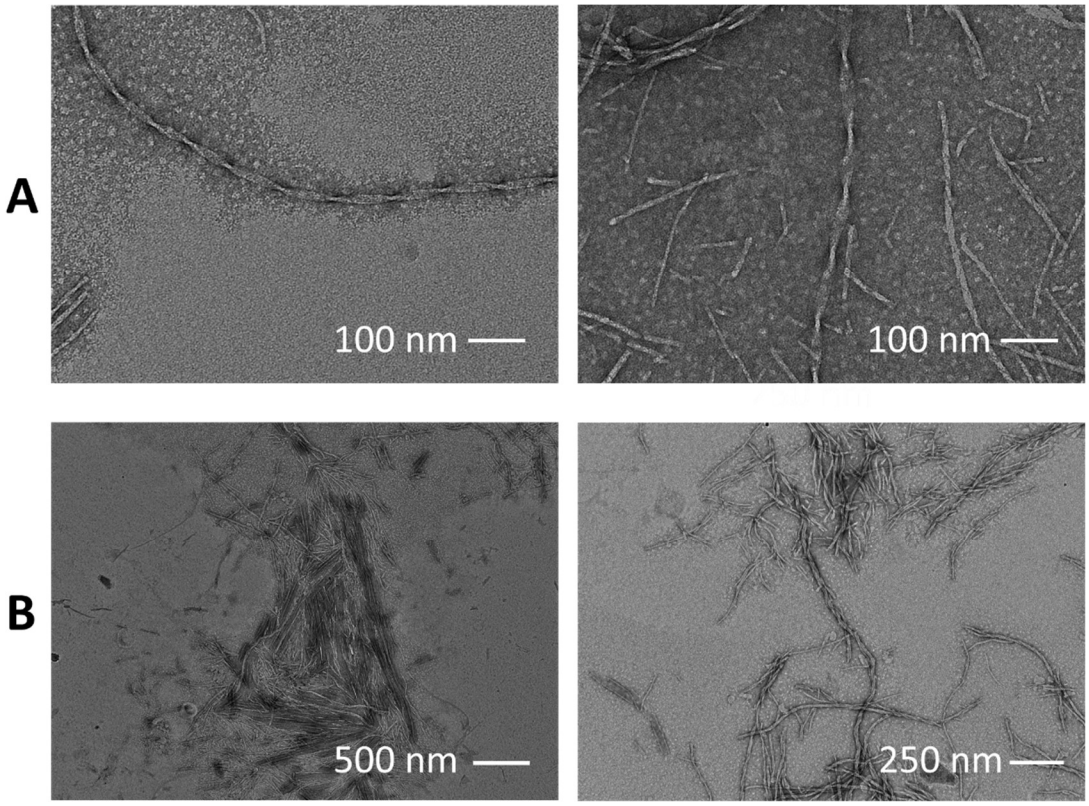

Figure 27. Representative TEM images of β-HA freshly annealed after assembly in pH2 (A) and pH4 (B) buffer. Generally the same twisted fibrils and aggregates were observed in both assembly conditions. The twisted fibrillar character is reminiscent of amyloid fibrils. Even among thin fibrils there is noticeable variation of width.

Conclusion:

The unexpected discovery of a water soluble self-assembling β-peptide from a mistaken sequence marks the first recorded instance of a β-peptide assembling polymorphically at a supramolecular level in aqueous buffer. Gellman A and Iso-A are the first reported instance of higher order self-assembly of a β-peptide into a nanotube[7], and β-HA verifies that unpredictable self-assembly of β-peptides at the tertiary and quaternary level can occur even with foldamers. In a mixed bag of results, the polymorphism of β-HA proves that β-peptides remain susceptible to unpredictable environmental influence. Hierarchical assembly of filaments forming sheets forming helical ribbons forming hollow tapes was documented, a process that was sped up by annealing once nucleation of helical ribbons occurred at room temperature.

Much like PP(R) from chapter 1, the heterogenous nature of β-HA's self-assembly makes cryo-EM structural characterization of individual supramolecular structures extremely difficult. Additionally, CD spectra indicated that the secondary structural characteristics of β-HA were distinctly different from the 14-helix, making characterization of the hierarchical sequence of assembly at lower level difficult to analyze or speculate about.

From comparison of sequence level differences between the soluble β-peptides: β-HA, Gellman A, and Iso-A, and the insoluble β-peptides: β-lys/ β-arg, a few remarks can be made. Soluble peptides all carried a net positive charge across the length of the peptide, and the global, vs. non-global distribution of positive charge did not alter the solubility of the resulting peptides. For any number of reasons, including the orientation of the sequence, the lack of ACHC residues, or the asymmetry of sidechain mediated salt bridges, β-HA does not prefer the 14-helical conformation in aqueous buffer. The insolubility of both uncapped β-lys and β-arg indicate that

affecting the acetylation of the N-terminus and amidation of the C-terminus does not improve solubility.

Further studies of the mechanical properties of β-HA, including its potential to form hydrogels or liquid crystals and optimization of assembly conditions to bias the formation of a single supramolecular structure could reveal more details about the mysterious properties of a peptide that appears to deviate from all previously understood paradigms of β-peptide self-assembly. Mutations of β-lys and β-arg to increase net charge, reverse sequence order, or truncate into a nonapeptide could help eliminate the observed solubility issues.

Chapter 3.1: Solving the Structure of a β-Peptide Foldamer Nanotube

Introduction:

Having taken a detour to explore the self-assembly properties of β-HA, the questions surrounding the supramolecular structure of the Gellman A remained unanswered. Failure to solubilize β-lys and β-arg meant no insight could be gained regarding the necessity of ACHC for 14-helix formation in aqueous conditions. We resolved to replicate the synthesis of Gellman A and characterize its structure using high-resolution Cryo-EM. At the time of writing, assignment of helical symmetry is currently being deliberated, so confirmation of results is not available.

Results and Discussion:

Peptide Synthesis and Assembly: Gellman A was synthesized according to procedures outlined by Pomerantz *et al*[8] to produce a lyophilized white powder. Gellman A was assembled initially at 3mg/mL in 10 mM pH4.0 acetate and Millipore water in ambient conditions. Aliquots were taken and annealed according to the following protocol in a thermal cycler: (1) rapid heating to 90 deg. C for 30 min and (2) cooling to 25 deg. C at a rate of 0.2 deg. C/min. No assemblies were observed on TEM after 1 day of assembly, so Gellman A was reassembled at 2%/w in Millipore water and in 10mM pH 4.0 acetate. Although Gellman A formed the expected population of nanotubes under TEM in both pH 4.0 acetate and Millipore water, visualization after freezing for cryo-EM imaging was difficult. Gellman A was assembled at 8%/w in 10mM pH 4.0 acetate resulting in the formation of an opaque white lyotropic liquid crystal phase which produced visible nanotubes after freezing.

Transmission Electron Microscopy: Assemblies of Gellman A at 2%/w in 10mM pH 4.0 acetate induced higher levels of nanotube formation than in Millipore water, although nanotubes could be seen in both conditions after 1 day of assembly at room temperature. (Figure 28.).

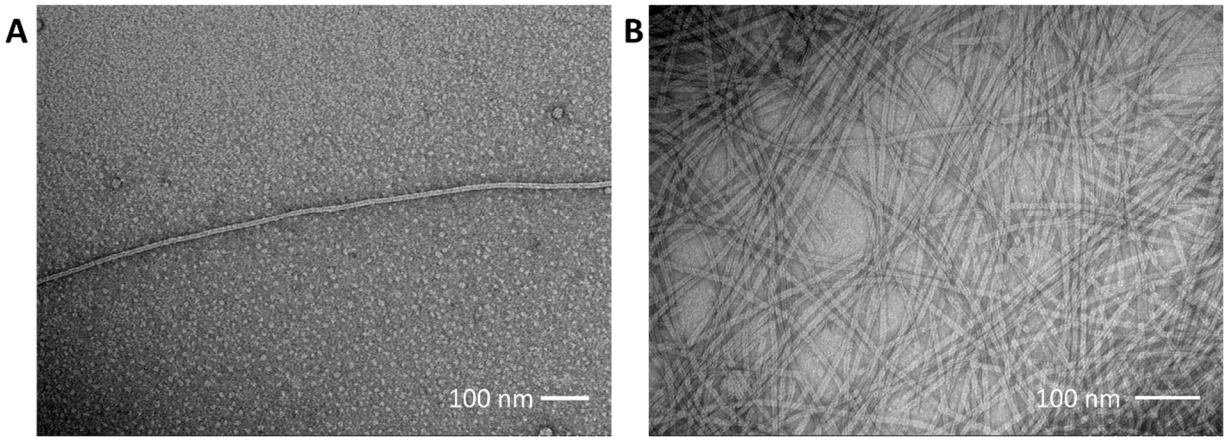

Figure 28. Representative TEM images of Gellman A assembled at 2%/w in Millipore water (A) and 10mM pH 4.0 acetate (B) at room temperature for 1 day. Images are stained with 1% UA. Solitary nanotubes formed throughout the Millipore water assembly, but dense collections of nanotubes were observed only in pH4 buffer.

Results of assembly match observations made by Pomerantz *et al*[7,8]. Tubes have a mean width of 10.977 nm with a standard deviation of 0.969 nm. A clearly visible lumen can be seen in isolated nanotubes with sufficient contrast.

Future Steps: Preliminary analysis of data collected from several hundred images of frozen nanotubes has given a rudimentary estimation of the electron densities associated with the nanotubes. One of the preliminary renders of the structure of Gellman A is shown (Figure 29.). This structure is not intended to be representative of the true resolution or structure of Gellman A but is nonetheless provided for closure.

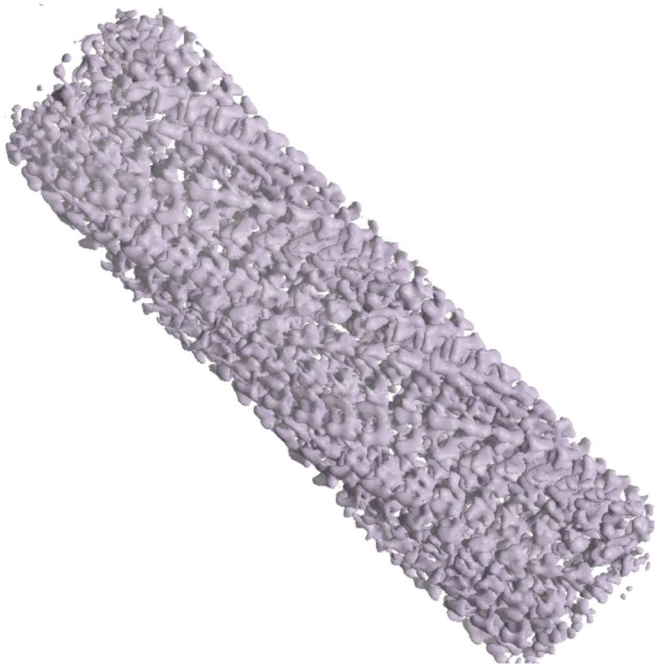

Figure 29. A possible depiction of the electron density of Gellman A. The start of structural analysis by high-resolution cryo-EM begins with refinement of raw averaged data! I am not qualified to tell you what this image means (yet) but it sure does look cool.

Materials and Methods:

Materials: All chemical reagents were purchased from Fisher Scientific, Inc. (Pittsburgh, PA), Anaspec, Inc (Fremont, CA) or Sigma-Aldrich Chemical Co. (St. Louis, MO) unless otherwise specified and used without further purification.

Peptide Synthesis and Purification: β^3-homologated and fmoc protected amino acids were purchased from Aapptec LLC (Louisville, KY). B-Peptides were synthesized on a .10 μmol scale using a CEM Liberty Blue microwave-assisted solid phase peptide synthesizer.

Capped β-peptides were synthesized as follows: Fmoc-protected amino acids were attached to a Rink Amide resin from CEM Co. (Matthews, NC) to produce a C-terminal amide. Standard Fmoc protection/deprotection chemistry was used with coupling cycles based on HBTU/Oxima activation protocols and base induced deprotection (20% piperidine in N, N-dimethylformamide with 0.1 M hydroxybenzotriazole) of Fmoc protecting group. All arginine groups were double coupled. Acetylation of the N-terminal (20% acetic anhydride in N, N-dimethylformamide) occurred with the final deprotection cycle.

Uncapped β-peptides were synthesized as follows: The first β-amino-acid was manually coupled to Wang Resin purchased from Aapptec LLC (Louisville, KY). Resin was swelled for 1hr with DIC at room temperature. Fmoc deprotection occurred using 20% piperidine in DMF for 5 minutes. 5 equiv of the first amino acid was coupled using HOAt (5 equiv) and DIC (5 equiv) in DMF for 15 minutes at room temperature. Successful coupling was verified using a Ninhydrin test. Manually coupled Wang resin was transferred to a microwave-assisted solid phase peptide synthesizer for automatic coupling of the remaining residues. Standard Fmoc protection/deprotection chemistry was used with coupling cycles based on HBTU/Oxima activation protocols and base induced deprotection (20% piperidine in N, N-dimethylformamide with 0.1 M hydroxybenzotriazole) of Fmoc protecting group. Arginine groups were double coupled. Acetylation of the N-terminus was omitted.

Gellman A was synthesized and assembled according to procedures outlined by Pomerantz *et al*.[8]

After synthesis, the coupled resin was washed with DMF and transferred to a Buchner funnel to be washed with acetone and dried in vacuo. The crude peptide was subjected to a cleavage protocol to separate it from the support resin using a solution of 92.5% trifluoroacetic

acid, 2.5% triisopropylsilane, 2.5% 3,6-Dioxa-1,8-octanedithiol, and 2.5% water. The cleavage solution was filtered and precipitated by centrifuge with cold diethyl ether (4ºC).

Peptides were purified with a Shimadzu LC-20AP preparatory reverse-phase HPLC with C18 column across a linear gradient of water/acetonitrile with 0.1% trifluoroacetic acid. Product identity was confirmed using mass spectrometry on a quadrupole time-of-flight mass spectrometer (Q-ToF Premier, Waters.) with electrospray ionization (ESI) in positive mode using Mass lynx software (V4.1). Product peaks were collected and dried in vacuo and lyophilized to yield a white powder.

Circular Dichroism: CD measurements were taken on a Jasco J-1500 CD Spectropolarimeter using a 0.20 mm quartz cuvette (Hellma USA Inc, Plainveiw, NY). Signals were measured three times consecutively, averaged, and corrected with a blank spectrum of the corresponding buffer. Spectra were taken with a scan rate of100nm/min from 190-260nm with a bandwidth of 2nm and data pitch of 0.2nm.

Negative Stain and TEM analysis: TEM grids were prepared with assembled samples of peptide at 3mg/mL concentration. 4µL of each sample were deposited onto 200-mesh carbon-coated copper grid (Electron Microscopy Services, Hatfield, PA) and allowed to incubate for 90 seconds. Excess liquid was wicked away and 4µL of 1% Uranyl Acetate solution was deposited onto the grid surface and incubated for 90 seconds. Remaining moisture was wicked away, and electron micrograph images were collected on a Hitachi HT-7700 transmission electron microscope. The microscope is equipped with a tungsten filament, an AMT CCD camera, and operates at an accelerating voltage of 80kV.

References:

1. Foldamers: A Manifesto, Samuel H. Gellman, Accounts of Chemical Research 1998 31 (4), 173-180, DOI: 10.1021/ar960298r
2. Romila D. Gopalan, Mark P. Del Borgo, Adam I. Mechler, Patrick Perlmutter, Marie-Isabel Aguilar, Geometrically Precise Building Blocks: the Self-Assembly of β-Peptides, Chemistry & Biology, Volume 22, Issue 11, 2015, Pages 1417-1423, ISSN 1074-5521, https://doi.org/10.1016/j.chembiol.2015.10.005.
3. Cheng RP, Gellman SH, DeGrado WF. beta-Peptides: from structure to function. Chem Rev. 2001 Oct;101(10):3219-32. doi: 10.1021/cr000045i. PMID: 11710070.
4. Raguse, T., Lai, J. and Gellman, S. (2002), Evidence that the β-Peptide 14-Helix is Stabilized by β3-Residues with Sidechain Branching Adjacent to the β-Carbon Atom. HCA, 85: 4154-4164. https://doi.org/10.1002/hlca.200290001
5. Hart SA, Bahadoor AB, Matthews EE, Qiu XJ, Schepartz A. Helix macrodipole control of beta 3 peptide 14-helix stability in water. J Am Chem Soc. 2003 Apr 9;125(14):4022-3. doi: 10.1021/ja029868a. PMID: 12670203.
6. Arvidsson, P.I., Rueping, L. & Seebach, D. Design, machine synthesis, and NMR-solution structure of a β-heptapetide forming a salt-bridge stabilised 314-helix in methanol and in water. Chem. Commun. (Camb.) 649–650 (2001).
7. Pizzey, C. L., Pomerantz, W. C., Sung, B. J., Yuwono, V. M., Gellman, S. H., Hartgerink, J. D., ... & Abbott, N. L. (2008). Characterization of nanofibers formed by self-assembly of β-peptide oligomers using small angle x-ray scattering. The Journal of chemical physics, 129(9), 09B603.

8. Pomerantz, W., Yuwono, V., Pizzey, C., Hartgerink, J., Abbott, N. and Gellman, S. (2008), Nanofibers and Lyotropic Liquid Crystals from a Class of Self-Assembling β-Peptides. Angewandte Chemie International Edition, 47: 1241-1244. https://doi.org/10.1002/anie.200704372
9. Armstrong, K. M., & Baldwin, R. L. (1993). Charged histidine affects alpha-helix stability at all positions in the helix by interacting with the backbone charges. Proceedings of the National Academy of Sciences of the United States of America, 90(23), 11337–11340. https://doi.org/10.1073/pnas.90.23.11337
10. Cheng RP, DeGrado WF. De novo design of a monomeric helical beta-peptide stabilized by electrostatic interactions. J Am Chem Soc. 2001 May 30;123(21):5162-3. doi: 10.1021/ja010438e. PMID: 11457373.
11. Alexander Fleming Discovery and Development of Penicillin - Landmark - American Chemical Society. (2022). Retrieved 1 April 2022, from https://www.acs.org/content/acs/en/education/whatischemistry/landmarks/flemingpenicillin.html
12. Édouard Bénédictus (October 1930), Glaces et verres; revue technique, artistique, pratique, 3 (18): 9.
13. French patent 405,881 (registered November 25, 1909).